J. Fluid Mech. (1989), *vol.* 199, *pp.* 519–540
Printed in Great Britain

A theoretical and experimental study of double-layer convection

By S. RASENAT, F. H. BUSSE AND I. REHBERG
Institute of Physics, University of Bayreuth, D-8580 Bayreuth, FRG

(Received 26 January 1988)

The onset of thermal convection in a double layer of two superimposed immiscible fluids heated from below is investigated. The linearized equations of the problem are analysed in a much wider region of the parameter space than has been studied before. It is shown that the onset of steady convection in the two layers may occur in the form of either viscously or thermally coupled motions. In addition to the oscillatory interfacial instability, which depends on a non-vanishing distortion of the interface, there exists another oscillatory instability which corresponds to a cyclic variation between viscous and thermal coupling. Conditions for the onset of this instability are outlined and its connections with the other modes of the system are demonstrated in bifurcation diagrams. In the experiments the shadowgraph method is used for the visualization of the onset of convection and for the measurement of its wavelength. Changeovers between viscous and thermal coupling can be identified, but the experimental realization of an oscillatory onset has been elusive so far.

1. Introduction

The problem of convection in two superimposed layers of immiscible liquids has received much attention in recent years. Originally most of the research was motivated by the suggested occurrence of two-layer convection in the Earth's mantle. The 670 km seismic discontinuity has been interpreted by some geophysicists as an interface separating two different types of mantle material. Richter & Johnson (1974) studied the dynamical implications of convection in superimposed layers of equal size and Busse (1981) investigated the case when the layers had quite different thickness. Further recent work on two-layer mantle convection has been described by Cserepes & Rabinowicz (1985) and Ellsworth & Schubert (1985). A laboratory study by Nguyen & Kulacki (1980) is also relevant.

Even without the possible application to mantle convection the problem of convection in superimposed layers has attracted considerable attention because of the possibility of Hopf bifurcations. While it can be shown that a single layer of fluid heated from below becomes unstable only through a monotonically growing instability, the possibility of overstable oscillations cannot be excluded in two superimposed layers. Indeed, a Hopf bifurcation was found by Gershuni & Zhukhovitskii (1982) even in the limit of negligible distortion of the interface. The distortion of the interface introduces an additional degree of freedom, and a Hopf bifurcation in this case had already been discussed by Richter & Johnson (1974). For more recent work on this topic we refer to Renardy & Joseph (1984) and to Renardy & Renardy (1985). The opportunity to investigate the nonlinear interaction between a Hopf bifurcation and a monotonic bifurcation or between two monotonic bifurcations has added to the appeal of the problem. A very recent nonlinear analysis

of an idealized version of the two-layer convection problem has been given by Proctor & Jones (1988).

Besides the numerous attractive features of the two-layer-convection problem, there are some less attractive properties which are in part responsible for the fact that it did not receive more attention in earlier years. First, there is the high-dimensional parameter space of the problem which has made it difficult to gain an overview over the manifold of solutions of the linear problem. Convection in a single layer of a Boussinesq fluid is governed by two dimensionless parameters, the Rayleigh and the Prandtl number, of which the latter drops out from the linear version of the problem. But of the order of ten non-dimensional parameters may be important in the two-layer problem. Some of those parameters, such as the Marangoni number for the interface or the ratio between the density difference of the fluids and the thermally induced density variation, can be eliminated from the problem by the consideration of special limits. But for the ratios of material properties there do not exist any preferred values.

Only a very small region of the parameter space is accessible in laboratory experiments. The experimental difficulties are compounded by the fact that there are few combinations of liquids that are truly immiscible. In most cases some diffusion of material occurs across the interface and the experiments have to be carried out in such a way that the timescale of the dynamic processes is short in comparison with timescale of the change of properties by the effects of diffusion. Nevertheless, there are a number of interesting features that can be realized in the laboratory. Careful measurements are highly desirable, especially with respect to nonlinear effects which are not readily accessible to theoretical analysis. Some initial attempts to obtain quantitative measurements of properties of two-layer convection will be reported at the end of this paper.

The primary goal of the theoretical analysis of this paper is a reasonably complete study of the linear problem of the onset of convection in superimposed layers. While it is impossible to derive plots of the critical conditions for all dimensionless parameters, the occurrence of interesting dynamical features can be traced in the parameter space. We are thus able, for example, to recognize the oscillatory solution of Gershuni & Zhukhovitskii (1982) as an intermediate form of convection between the viscous and thermal coupling cases. A guiding principle for our analysis is the property that both layers are close to instability by overturning motions since the corresponding part of the parameter space is the most likely one to offer new features. The remaining, and far larger, part of the parameter space probably does not deviate much from the case of ordinary single-layer convection in that convection occurs in one of the layers while the stable second layer plays a passive role.

The paper starts with the mathematical formulation of the problem in §2. Distortions of the interface will be neglected until §5. In §3 the competition between viscous and thermal coupling is described, and in §4 the oscillatory modes are analysed as a special feature of this competition. Another type of oscillation becomes possible when distortions of the interface are included in the analysis as is done in §5. A laboratory experiment is described in §6 and some measurements are reported in §7. The concluding remarks summarize the progress that has been achieved and provide an outlook on future work.

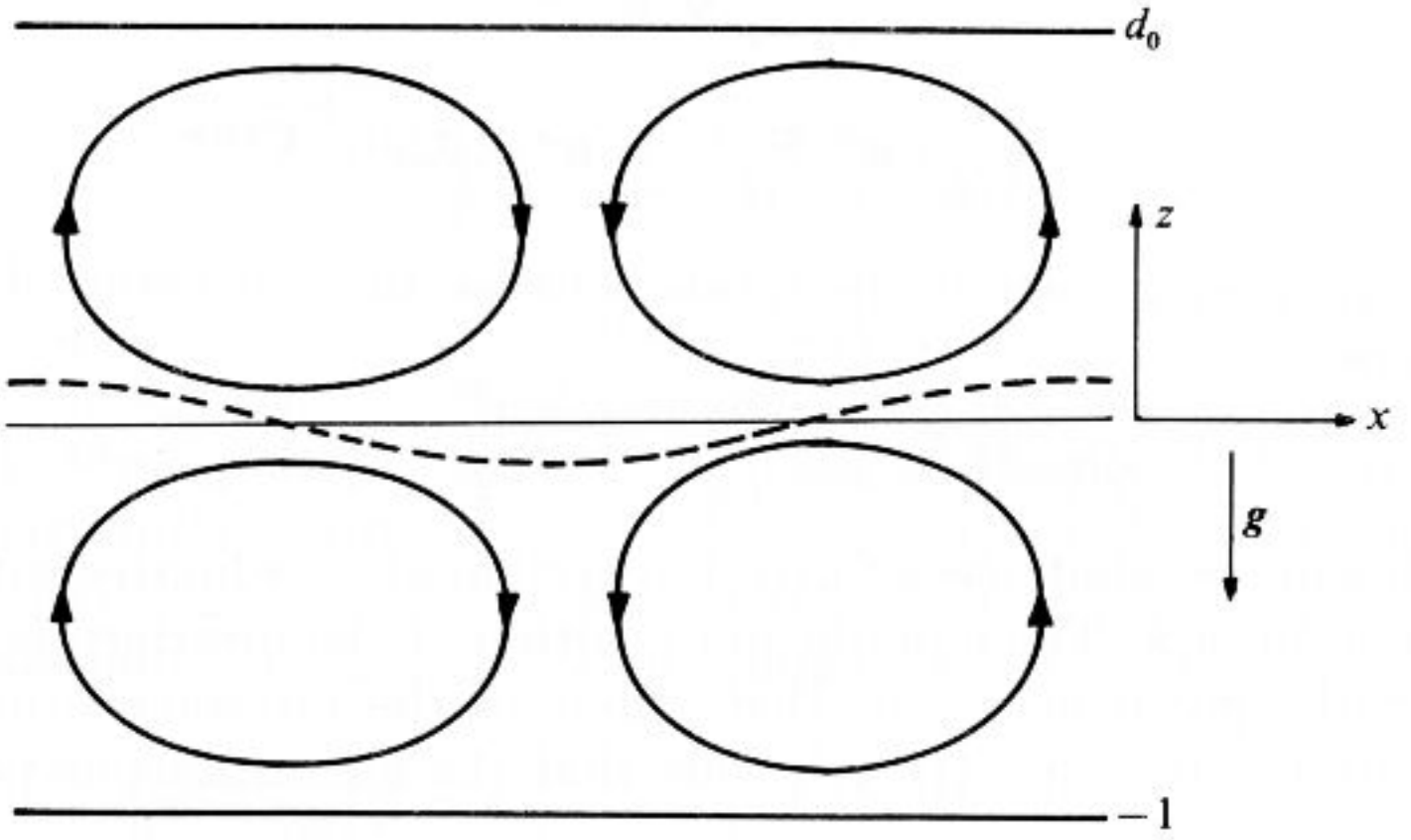

FIGURE 1. Geometrical configuration of the problem, with streamlines indicating a case of thermal coupling.

2. Mathematical formulation of the problem

We consider two horizontal fluid layers with the lighter fluid of density ρ^* on the top of the heavier fluid with the density ρ as shown in figure 1. Using the thickness d of the latter fluid as lengthscale, d^2/κ as timescale and βd as scale of the temperature, we obtain for the lower layer a dimensionless form of the equations governing the velocity vector $\boldsymbol{u}$ and the deviation θ of the temperature from its static distribution:

$$P^{-1}\left(\frac{\partial}{\partial t}+\boldsymbol{u}\cdot\boldsymbol{\nabla}\right)\boldsymbol{u}=-\boldsymbol{\nabla}\pi+Rk\theta+\nabla^2\boldsymbol{u}, \tag{2.1a}$$

$$\boldsymbol{\nabla}\cdot\boldsymbol{u}=0, \tag{2.1b}$$

$$\left(\frac{\partial}{\partial t}+\boldsymbol{u}\cdot\boldsymbol{\nabla}\right)\theta=\boldsymbol{u}\cdot\boldsymbol{k}+\nabla^2\theta. \tag{2.1c}$$

The constants κ and β denote the thermal diffusivity and the absolute value of the static temperature gradient. We have assumed a Boussinesq fluid in that the variation of density with temperature,

$$\hat{\rho}=\rho(1-\gamma(T-T_0)), \tag{2.2}$$

is taken into account only in the gravity term. All terms that can be written as gradients in the equation of motion (2.1a) have been combined in the term $\boldsymbol{\nabla}\pi$. The vertical unit vector $\boldsymbol{k}$ is directed opposite to gravity and the Rayleigh and Prandtl numbers are defined by

$$R=\frac{\gamma g\beta d^4}{\nu\kappa}, \quad P=\frac{\nu}{\kappa}, \tag{2.3}$$

where ν is the kinematic viscosity of the lower fluid and g is the acceleration due to gravity. Using the same scales we can write the equations for the dimensionless velocity vector $\boldsymbol{u}^*$ and for the dimensionless deviation θ^* of the temperature from its static distribution in the upper fluid layer in the form

$$P^{-1}\left(\frac{\partial}{\partial t}+\boldsymbol{u}^*\cdot\boldsymbol{\nabla}\right)\boldsymbol{u}^*=-\boldsymbol{\nabla}\pi^*/\rho_0+\gamma_0 Rk\theta^*+\nu_0\nabla^2\boldsymbol{u}^*, \tag{2.4a}$$

$$\boldsymbol{\nabla}\cdot\boldsymbol{u}^* = 0, \tag{2.4b}$$

$$\left(\frac{\partial}{\partial t}+\boldsymbol{u}^*\cdot\boldsymbol{\nabla}\right)\theta^* = \boldsymbol{u}^*\cdot\boldsymbol{k}\beta_0+\kappa_0\nabla^2\theta^*, \tag{2.4c}$$

where γ_0, ν_0, β_0, κ_0, ρ_0 denote the ratios between the properties of the upper and the lower layers,

$$\gamma_0 \equiv \frac{\gamma^*}{\gamma}, \quad \nu_0 \equiv \frac{\nu^*}{\nu} \equiv \frac{\mu_0}{\rho_0}, \quad \beta_0 \equiv \frac{\beta^*}{\beta}, \quad \kappa_0 \equiv \frac{\kappa^*}{\kappa}, \quad \rho_0 \equiv \frac{\rho^*}{\rho}. \tag{2.5}$$

In the following we shall use a Cartesian system of coordinates with the z-coordinate in the direction of $\boldsymbol{k}$. The equilibrium position of the interface between the fluids is assumed to be given by $z = 0$. Distortions of the interface from this position are described by the function $\zeta(x, y, t)$ such that the instantaneous position is given by

$$F(x, y, z, t) \equiv z-\zeta = 0. \tag{2.6}$$

The kinematic condition for the material interface, $\mathrm{D}F/\mathrm{D}t = 0$, yields two equations for ζ:

$$\frac{\partial}{\partial t}\zeta-\boldsymbol{u}\cdot\boldsymbol{k}+\boldsymbol{u}\cdot\boldsymbol{\nabla}\zeta = 0, \quad \frac{\partial}{\partial t}\zeta-\boldsymbol{u}^*\cdot\boldsymbol{k}+\boldsymbol{u}^*\cdot\boldsymbol{\nabla}\zeta = 0. \tag{2.7}$$

The outer boundaries of the double layer are located at $z = -1$ and at $z = d_0$. For simplicity we shall assume no-slip conditions at these boundaries together with fixed temperatures,

$$u_z = \partial_z u_z = \theta = 0 \quad \text{at} \quad z = -1, \qquad u_z^* = \partial_z u_z^* = \theta^* = 0 \quad \text{at} \quad z = d_0, \tag{2.8}$$

where the condition for the tangential component of the velocity has been transformed into a condition on the vertical component with the help of the equation of continuity.

Since we are restricting the attention in this paper to the onset of infinitesimal disturbances we can neglect the terms $\boldsymbol{u}\cdot\boldsymbol{\nabla}\boldsymbol{u}$, $\boldsymbol{u}\cdot\boldsymbol{\nabla}\theta$ and $\boldsymbol{u}\cdot\boldsymbol{\nabla}\zeta$ and the analogous terms for the upper layer in (2.1), (2.4) and (2.7). Without losing generality we may write the solution in the form

$$(u_z, u_z^*, \theta, \theta^*, \zeta) = (\phi(z), \phi^*(z), \tau(z), \tau^*(z), \zeta_0)\exp(\mathrm{i}\alpha x+\sigma t). \tag{2.9}$$

Because of the horizontal isotropy of the layer, three-dimensional solutions will yield the same eigenvalue σ as the two-dimensional solution (2.9) as long as the horizontal wavevectors have the same absolute value α. By taking the z-component of the curlcurl of (2.1) and (2.4) we obtain

$$\left(\frac{\partial^2}{\partial z^2}-\alpha^2-\sigma P^{-1}\right)\left(\frac{\partial^2}{\partial z^2}-\alpha^2\right)\phi = R\alpha^2\tau, \quad \left(\frac{\partial^2}{\partial z^2}-\alpha^2-\sigma\right)\tau = -\phi, \tag{2.10a}$$

$$\left(\frac{\partial^2}{\partial z^2}-\alpha^2-\frac{\sigma P^{-1}}{\nu_0}\right)\left(\frac{\partial^2}{\partial z^2}-\alpha^2\right)\phi^* = \frac{R\gamma_0\alpha^2\tau^*}{\nu_0}, \quad \left(\frac{\partial^2}{\partial z^2}-\alpha^2-\frac{\sigma}{\kappa_0}\right)\tau^* = -\frac{\beta_0\phi^*}{\kappa_0}. \tag{2.10b}$$

The kinematic condition (2.7) at the interface becomes

$$\sigma\zeta_0 = \phi = \phi^* \quad \text{at} \quad z = 0. \tag{2.11a}$$

The continuity of the temperature, the heat transport and the tangential velocity require the conditions

$$-\zeta_0+\tau = -\beta_0\zeta_0+\tau^* \quad \text{at} \quad z = 0, \tag{2.11b}$$

$$\frac{\partial}{\partial z}\tau = \lambda_0 \frac{\partial}{\partial z}\tau^* \quad \text{at} \quad z = 0, \tag{2.11c}$$

$$\frac{\partial}{\partial z}\phi = \frac{\partial}{\partial z}\phi^* \quad \text{at} \quad z = 0, \tag{2.11d}$$

where the equation of continuity has been used for the derivation of condition (2.11*d*). The ratio of λ_0 of the thermal conductivities between the upper and lower layers is usually equal to β_0^{-1}. But in the case of mantle convection only the superadiabatic part of the temperature gradient enters β_0 and thus λ_0 and β_0 may be independent. In deriving the equation for the continuity of the tangential stress we must take into account the variation with temperature T of the surface tension Σ,

$$\left(\alpha^2 + \frac{\partial^2}{\partial z^2}\right)\phi = \mu_0 \left(\alpha^2 + \frac{\partial^2}{\partial z^2}\right)\phi^* - M(\theta - \zeta)\,\alpha^2, \tag{2.11e}$$

where the Marangoni number M is defined by

$$M \equiv -\frac{\mathrm{d}\Sigma}{\mathrm{d}T}\frac{\beta d^2}{\nu\kappa\rho}.$$

The continuity of the normal stress requires

$$\frac{1}{\alpha^2}\left(\frac{\partial^2}{\partial z^2} - 3\alpha^2 - \sigma P^{-1}\right)\frac{\partial}{\partial z}\phi = \mu_0 \frac{1}{\alpha^2}\left(\frac{\partial^2}{\partial z^2} - 3\alpha^2 - \frac{\sigma P^{-1}}{\nu_0}\right)\frac{\partial}{\partial z}\phi^* + \left[\frac{\rho - \rho^*}{\rho\gamma\beta d}R + \alpha^2 S\right]\zeta_0, \tag{2.11f}$$

where S is the dimensionless surface tension,

$$S = \Sigma d/\nu\rho\kappa.$$

In order to avoid the distinction between the ratios of kinematic and dynamic viscosities, we shall assume that the density difference across the interface, $\rho - \rho^*$, is small. This assumption does not contradict the fact that the ratio $(\rho - \rho^*)/\rho\gamma\beta d$ is large in typical laboratory situations, since the relative change in density owing to thermal expansion rarely exceeds 10^{-3}. For this reason and because of the additional stabilizing influence of surface tension, the bracket multiplying ζ_0 is usually large with the consequence that the distortion ζ_0 has a negligible effect on the dynamics of double-layer convection. In §3 and 4 the limit of vanishing ζ_0 will thus be assumed. We shall return to the case of finite ζ_0 in §5.

Equations (2.10) together with the boundary conditions (2.8) and the matching conditions (2.11) at $z = 0$ can be solved by the shooting method. Three independent solutions $\phi_n(z)$, $\phi_n^*(z)$, $n = 1, 2, 3$, of (2.10) can be obtained by integrating numerically towards $z = 0$ from $z = -1$ and $z = d_0$, respectively, because there are three independent choices of the unspecified boundary conditions possible at the initial points $z = -1$ and $z = d_0$. The correct solution satisfying the matching conditions as well can be represented as a superposition of the three independent solutions in each layer:

$$\phi(z) = \sum_n A_n \phi_n(z), \quad \phi^*(z) = \sum_n B_n \phi_n^*(z).$$

The six matching conditions (2.11) provide six linear homogeneous equations for the coefficients A_n, B_n which are solvable if and only if σ is an eigenvalue. Since we are interested in the case of marginal stability we replace σ by $\mathrm{i}\omega$ and regard R as the real

part of the eigenvalue instead of the real part of σ. The lowest value $R_0(\alpha)$ of R as a function of α for which solutions exist will be considered in the following. Of particular interest is the absolute minimum of $R_0(\alpha)$ since it describes the critical value of the Rayleigh number at which the onset of convection must be expected.

A Runge–Kutta scheme has been used for the numerical integration of (2.10). For each of the intervals, $-1 \leqslant z \leqslant 0$ and $0 \leqslant z \leqslant d_0$, 50 steps were typically used. Comparisons with computations based on 25 and 100 steps indicate an accuracy of about three digits for the solutions. The zeros of the determinant of the linear equations for the unknowns A_n, B_n have been obtained with a Newton–Raphson iteration method. In the case of steady onset of convection, $\omega = 0$, the determinant is real and its zero determines the eigenvalue $R_0(\alpha)$. Oscillatory onset of convection, $\omega \neq 0$, leads to a complex determinant, the real and imaginary parts of which must vanish. These two conditions yield the values for $R_0(\alpha)$ and $\omega(\alpha)$.

3. Onset of convection with viscous and thermal coupling

In addition to the neglect of the distortion ζ_0 of the interface and the assumption of nearly equal densities of the two fluids we introduce some further simplifications in order to reduce the dimension of the parameter space. Since Marangoni effects become important in comparison to buoyancy forces only if the thickness of the layers becomes sufficiently small, it is possible to consider the limit $M \approx 0$ in which case the number of parameters of the problem is decreased by one. The opposite limit, of dominating Marangoni effect and vanishing buoyancy force, has been considered by Zeren & Reynolds (1972). These authors also mention that the Marangoni effect is often much diminished because of the presence of small impurities at the surface. It thus seems to be justified to consider the problem without this effect. Since the specific heat of various liquids does not vary much and since it appears to have little influence on the dynamics of the problem it seems appropriate to set the ratio c^*/c equal to unity with the result $\lambda_0 = \kappa_0$. Since we shall also assume $\beta_0 = \kappa_0^{-1}$ unless indicated otherwise, our task has thus been reduced to the problem of determining the critical conditions as a function of the parameters d_0, γ_0, κ_0, μ_0 and P. In this section we shall restrict the attention to the onset of stationary convection, in which case the Prandtl number P does not enter the analysis.

It is convenient to introduce a separate Rayleigh number R^* for the upper layer, which is defined by

$$R^* \equiv R\gamma_0 d_0^4/\kappa_0^2\mu_0. \tag{3.1}$$

The ratio R^*/R provides a measure for the ratio of the contributions from the two layers to the buoyancy-driven instability. When this ratio is significantly different from unity, the onset of instability occurs primarily in one layer while the other layer plays a passive role. Motions in the latter layer are weak and are driven primarily through viscous coupling at the interface. Even in the case $R \approx R^*$ one of the two layers may play a passive role if d_0 is either large or small compared with unity since the optimal wavenumbers are very different for the two layers. In this case, however, some novel features may occur which will be discussed in the next section in connection with the oscillatory onset of convection.

A typical case in which both layers provide the same contribution to the buoyancy-driven instability is given by two fluids with nearly the same properties and with $d_0 = 1$. The critical Rayleigh number for this case is well known (Pellew &

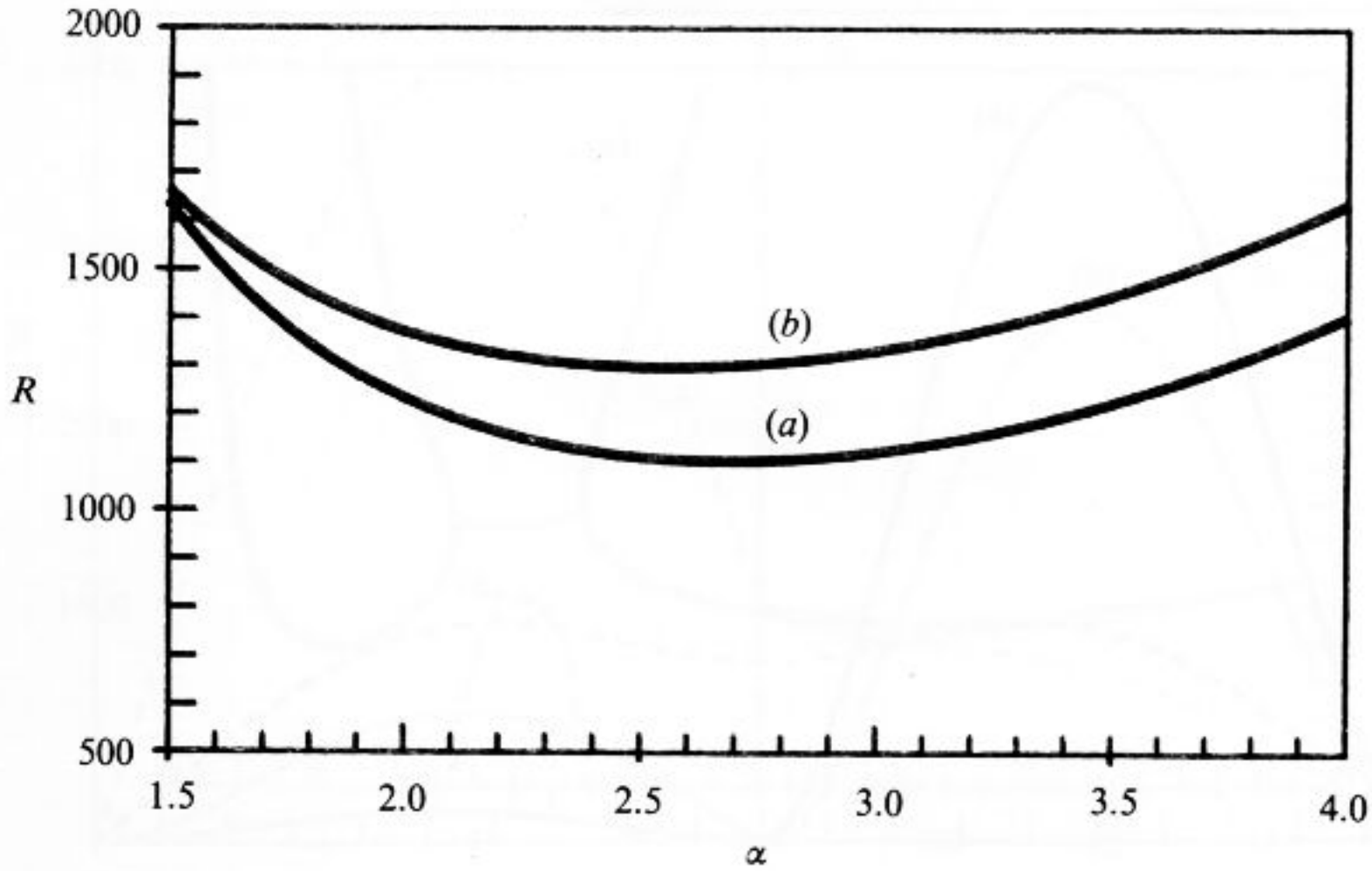

FIGURE 2. Two layers with the same material properties superimposed, $\gamma_0 = \mu_0 = \kappa_0 = d_0 = \beta_0 = 1$. The curves describe the onset of convection with (*a*) viscous, and (*b*) thermal coupling.

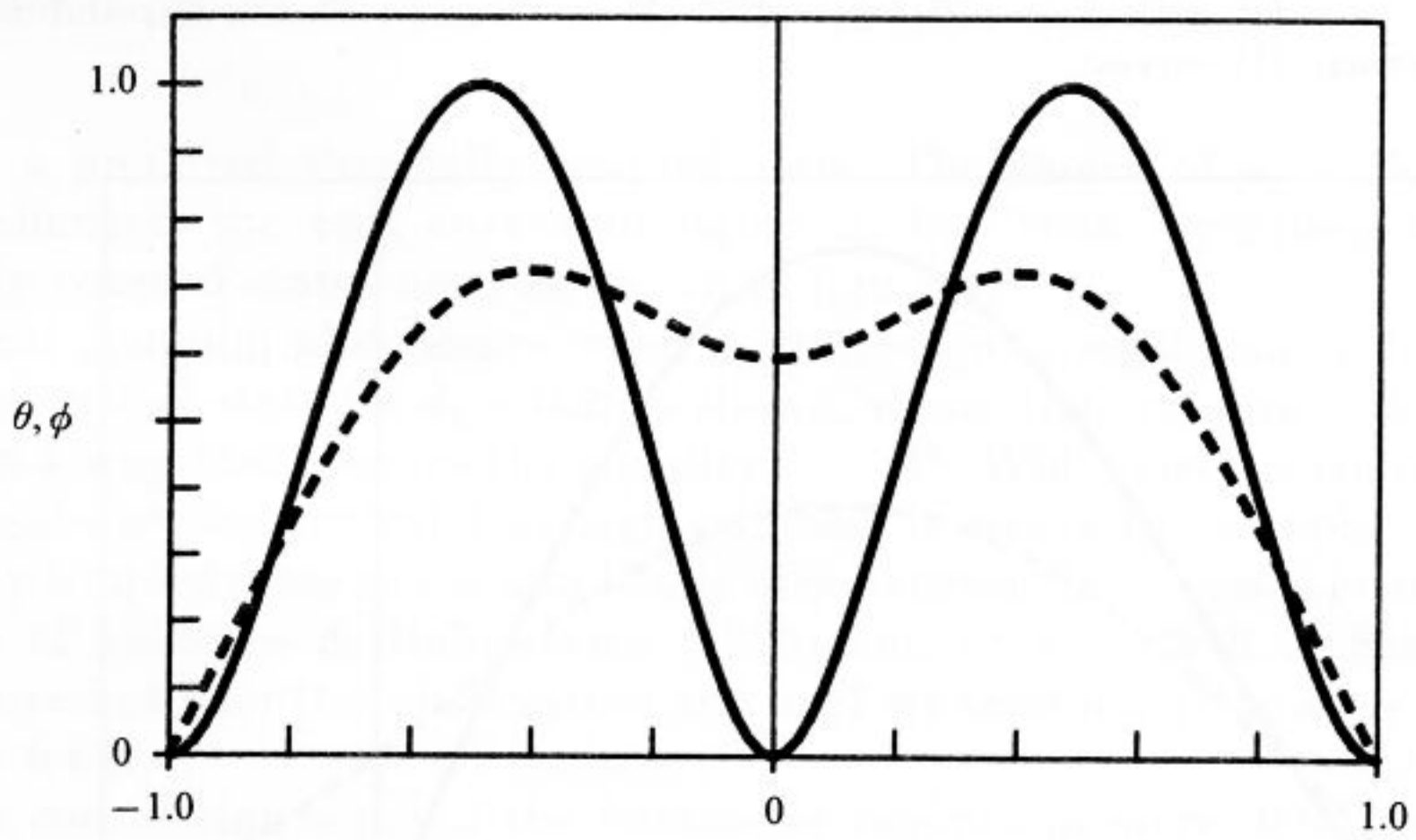

FIGURE 3. The functions $\phi(z)$ (solid) and $\theta(z)$ (dashed) for the thermal coupling case of figure 2 for $\alpha = 2.5$, $R = 1296$.

Southwell 1940) since it corresponds to that of a single layer with a rigid and a stress-free boundary:

$$R_c = 1101, \quad \alpha_c = 2.67. \tag{3.2}$$

In addition to this eigenvalue, which corresponds to the minimum of curve (*a*) in figure 2, there is another slightly higher eigenvalue given by curve (*b*) of figure 2. While the critical Rayleigh number (3.2) is associated with an antisymmetric function $\phi(z)$ (here and in the following we replace ϕ^* by $\phi(z)$ with $z > 0$), curve (*b*) corresponds to a symmetric function $\phi(z)$ as shown in figure 3. Since the temperature field $\theta(z)$ does not change sign, the convection motion in the two layers is thermally coupled in this case, in contrast to the normal viscous coupling. The main difference between the viscously coupled and the thermally coupled state is expressed in the

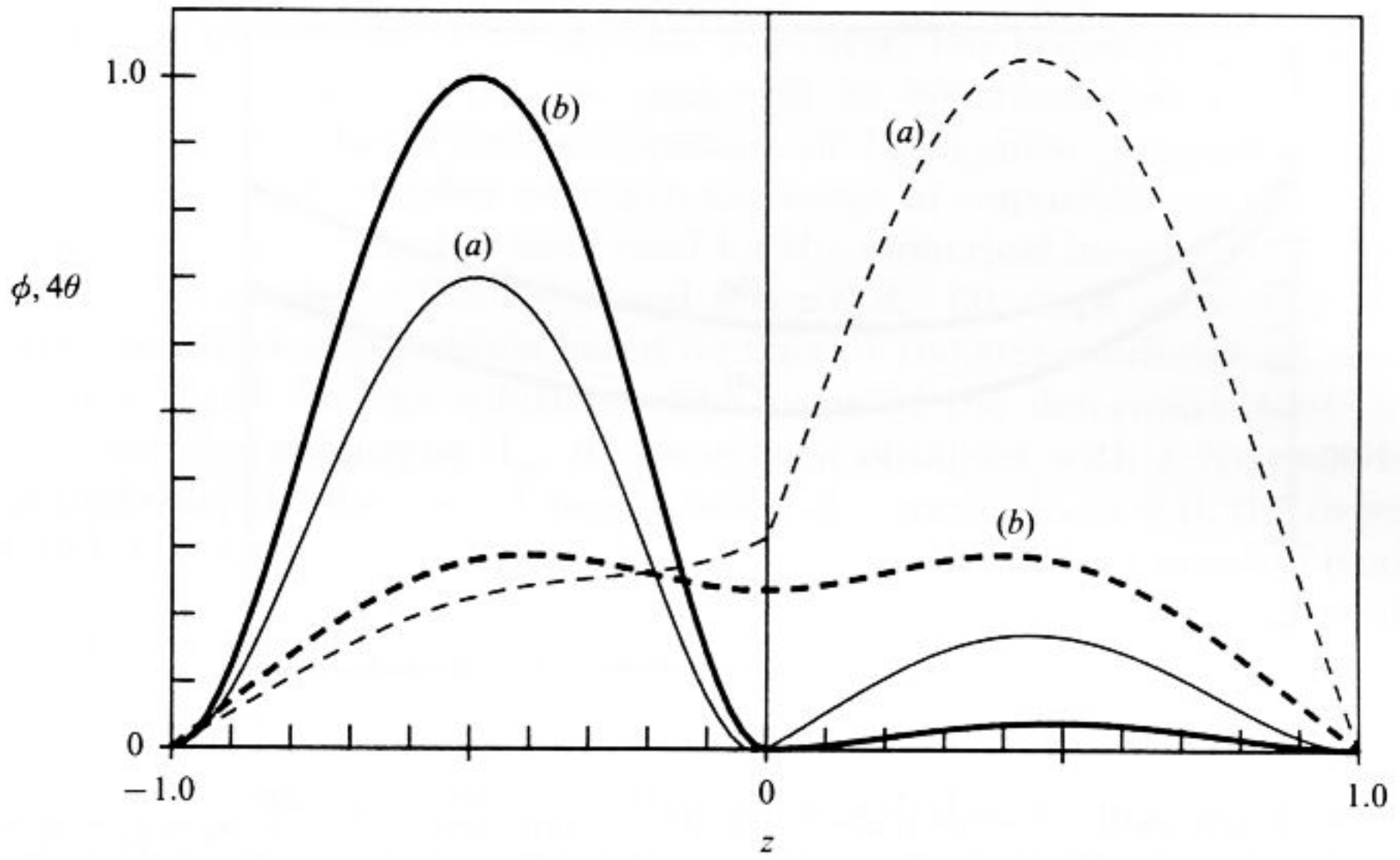

FIGURE 4. Eigenfunctions $\phi(z)$ (solid) and $\theta(z)$ (dashed) for two branches in the case $\gamma_0 = d_0 = 1$, $\kappa_0 = 0.2$, $\mu_0 = 25$, $R = R^*$ with $R_c = 1101$, $\alpha_c = 2.67$ (lower branch, (*a*) curves) and $R = 1296$, $\alpha = 2.6$ (upper branch, (*b*) curves).

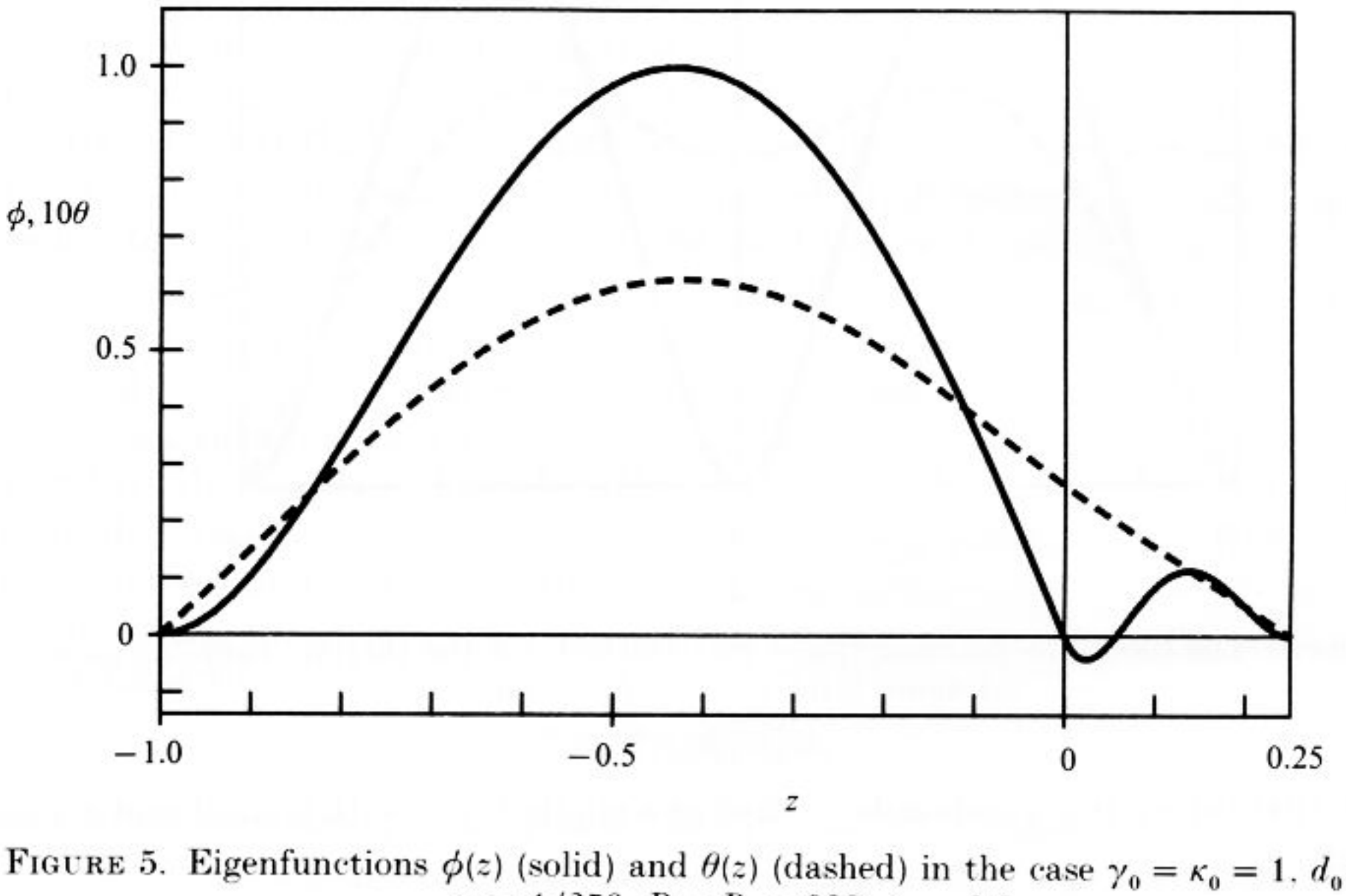

FIGURE 5. Eigenfunctions $\phi(z)$ (solid) and $\theta(z)$ (dashed) in the case $\gamma_0 = \kappa_0 = 1$, $d_0 = 0.25$, $\mu_0 = 1/256$, $R = R_c = 928$, $\alpha_c = 2.6$.

sign of the vorticity. While in the former state the rolls have the opposite sense of circulation, the vorticity has the same sign on both sides of the interface in the thermally coupled case. This condition is often satisfied in an average sense only since a small third counter-rotating roll may develop near the interface. But this property does not change the fact that there are two basically different types of coupling between superimposed layers.

It may appear that thermal coupling is a rare event and that viscous coupling is usually preferred, as in the case of figure 2. But a small change of the parameters

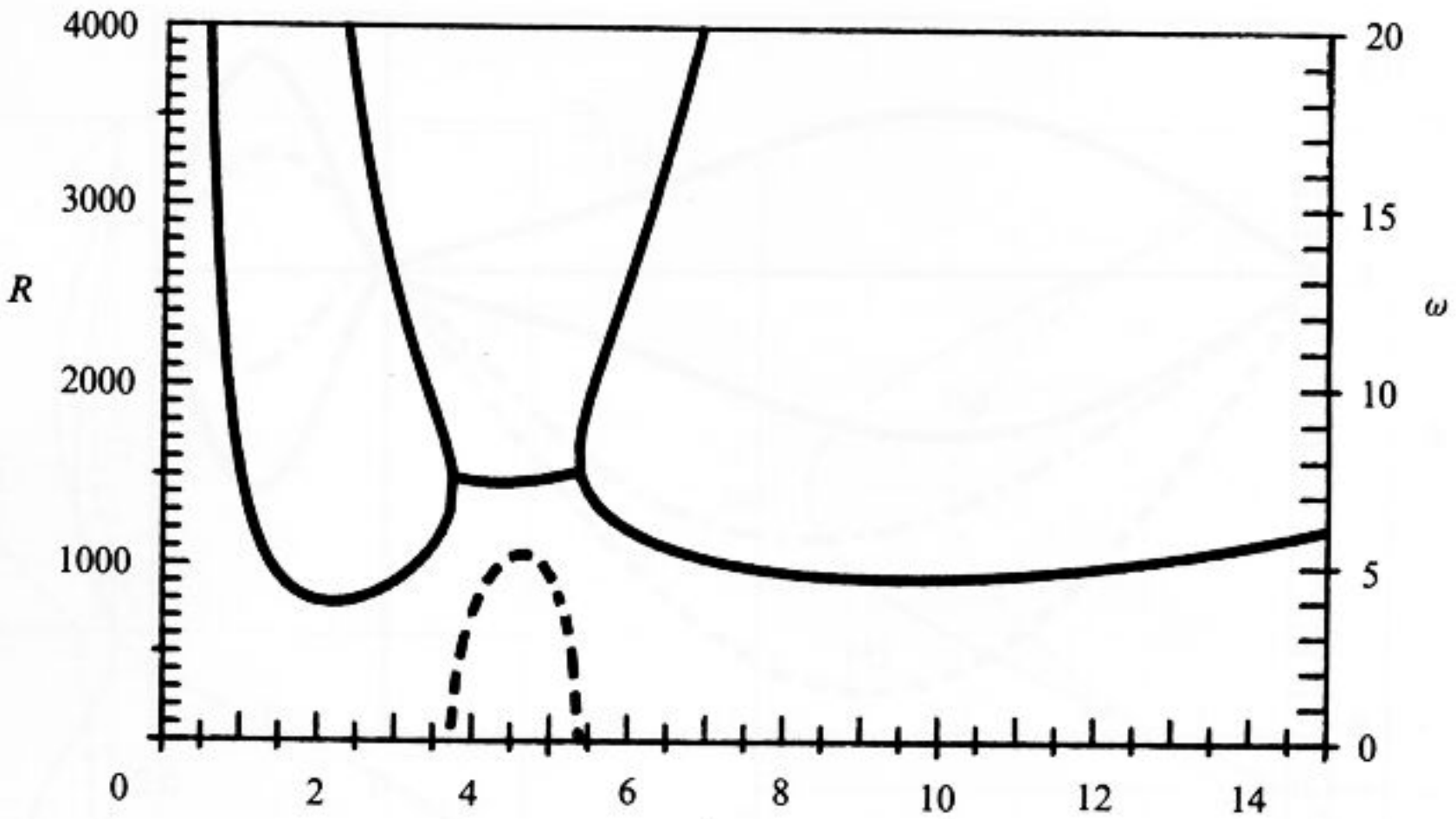

FIGURE 6. Neutral curves $R(\alpha)$ for the case of Busse (1981), $\gamma_0 = \kappa_0 = P = 1$, $\mu_0 = 0.1$, $d_0 = 0.25$, $\beta_0 = 25$, with stress-free conditions at $z = -1, d_0$. For the Hopf bifurcation branch the frequency ω is given by the dashed curve (scale on the right side).

leads to a preferred thermally coupled state. The choice of $\mu_0 = 25$, $\kappa_0 = 0.2$ has hardly changed the two curves in figure 2, but both eigenfunctions represent thermally coupled states now, as shown in figure 4.

Thermal coupling also occurs when d_0 differs quite significantly from unity. In figure 5 a critical state for $d_0 = 0.25$ is shown, where the properties have again been chosen in a way that ensures the equality $R = R^*$. While viscous coupling may still predominate at the critical Rayleigh number, it seems to be replaced often by a thermally coupled state as the amplitude of convection increases. The fully nonlinear analyses of Cserepes & Rabinowicz (1985) and of Ellsworth & Schubert (1985) provide examples for this observation and in §7 we shall report on some experimental evidence for it.

Before considering some of the parameter regimes in more detail we discuss the onset of oscillations as an intermediate state between the states of viscous and thermal coupling.

4. Convection in the form of the oscillatory coupling instability

Oscillatory modes in the form of propagating gravity or capillary waves at the interface form a prominent part of the solution spectrum of (2.10) and (2.11) when a distortion ζ_0 is admitted. Their influence on the convective instability will be discussed in the next section. Oscillatory modes with vanishing distortion are less obvious, and their appearance in the analysis of Gershuni & Zhukhovitskii (1982) was registered with surprise. It is not clear from the latter paper that a Hopf bifurcation will ever correspond to the point of marginal stability.

In the paper of Busse (1981) two-layer convection with $\omega = 0$ was investigated for stress-free outer boundaries, i.e. $\partial^2_{zz} u_z = 0$ at $z = -1$ and at $z = d_0$. In the case $d_0 = 0.25$, $\mu_0 = 0.1$, $\gamma_0 = \kappa_0 = 1$, $R^* = 125R/128$ it was noticed that no steady onset convection existed within an intermediate range of wavenumbers. The open question of an oscillatory onset has led to a new analysis of the problem. Indeed, as shown in figure 6 there is a Hopf bifurcation branch connecting the two monotonic branches

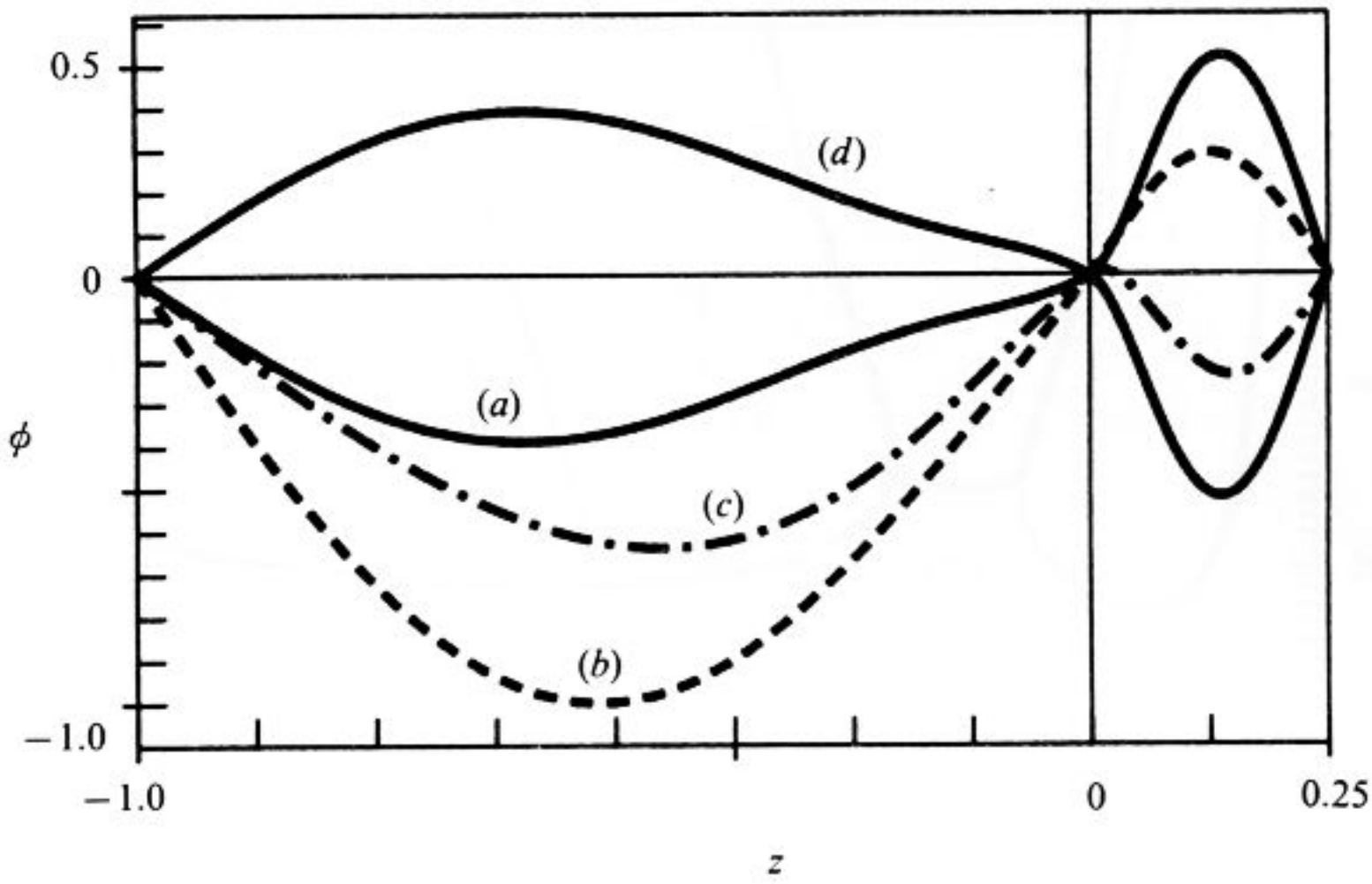

FIGURE 7. Eigenfunction $\phi(z)$ for the case of figure 6 at $R = 1463$, $\alpha = 4.5$ with $\omega = 5.22$. The curves (a), (b), (c), (d) describe $\phi(z)$ at the times $t = 0$, $\pi/3\omega$, $2\pi/3\omega$, π/ω, respectively. The thermal coupling phase is evident in case (c).

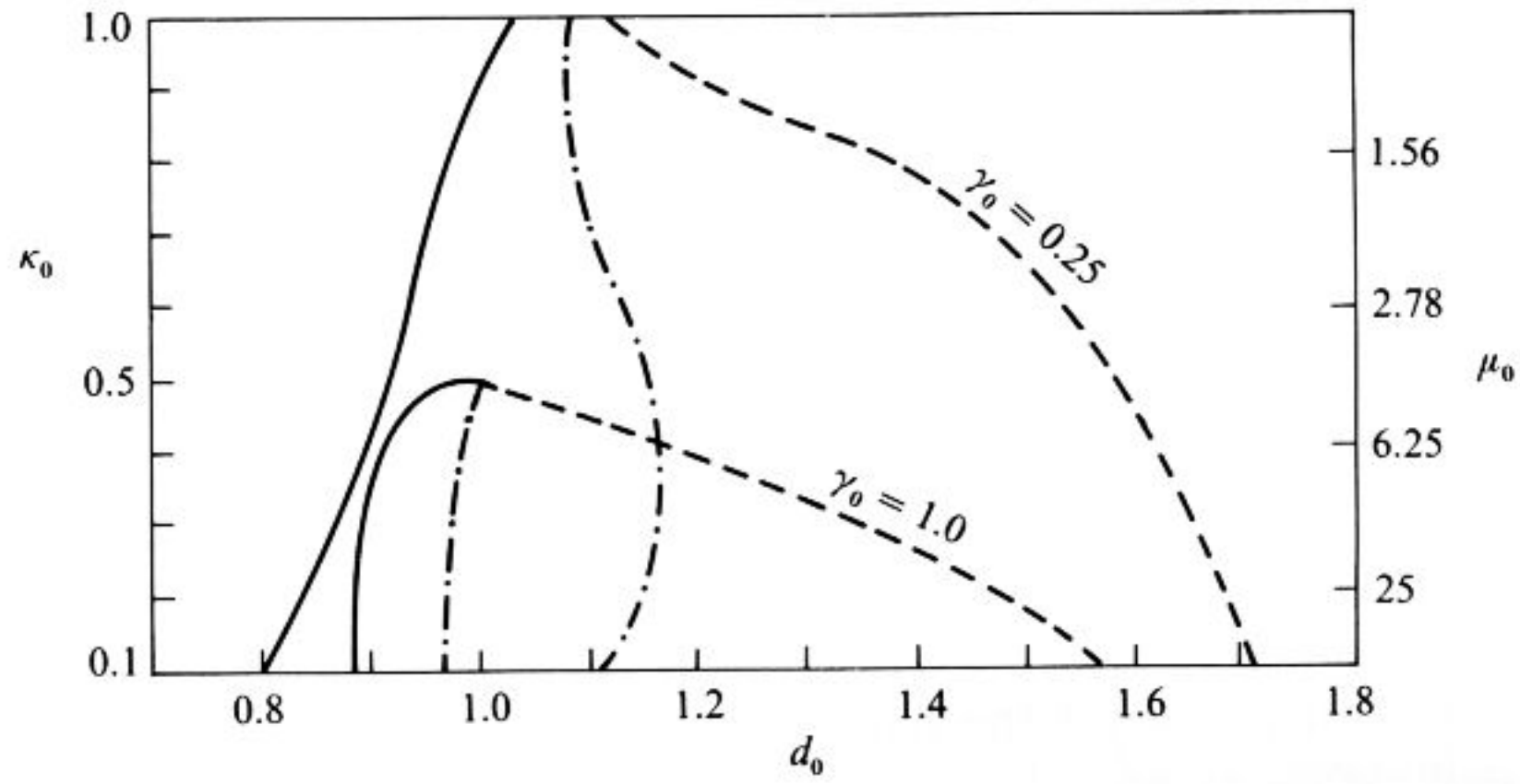

FIGURE 8. Approximate boundaries between the regimes of viscous coupling and oscillatory coupling (solid lines), between oscillatory coupling and thermal coupling (dash-dotted lines) and between thermal and viscous coupling (dashed lines). Two cases are shown, $\gamma_0 = 0.25$ and 1.0. Increasing γ_0 corresponds to decreasing domains of oscillatory coupling. The scale for μ_0 on the right side applies for $\gamma_0 = 1$; the scale must be multiplied by γ_0 in the other case. The other parameters are chosen such that $R = R^*$ holds for $d_0 = 1$.

which describe the onset of convection, with high and low wavenumbers predominating in the upper and lower layers, respectively. The structure of the eigenfunction, as indicated in figure 7, clearly indicates that the Hopf bifurcation represents an alternating viscous and thermal coupling process. Because of the phase shift of about 60° in the motions on both sides of the interface, the superimposed rolls exhibit the same sense of circulation during a significant part of the cycle. Nearly the same diagrams as shown in figures 6 and 7 have been obtained for rigid boundaries at $z = -1$, d_0 (Rasenat 1987).

The Hopf bifurcation in the case $d_0 = 0.25$ is of lesser interest since the critical Rayleigh number is given by the monotonic branches. The oscillatory coupling

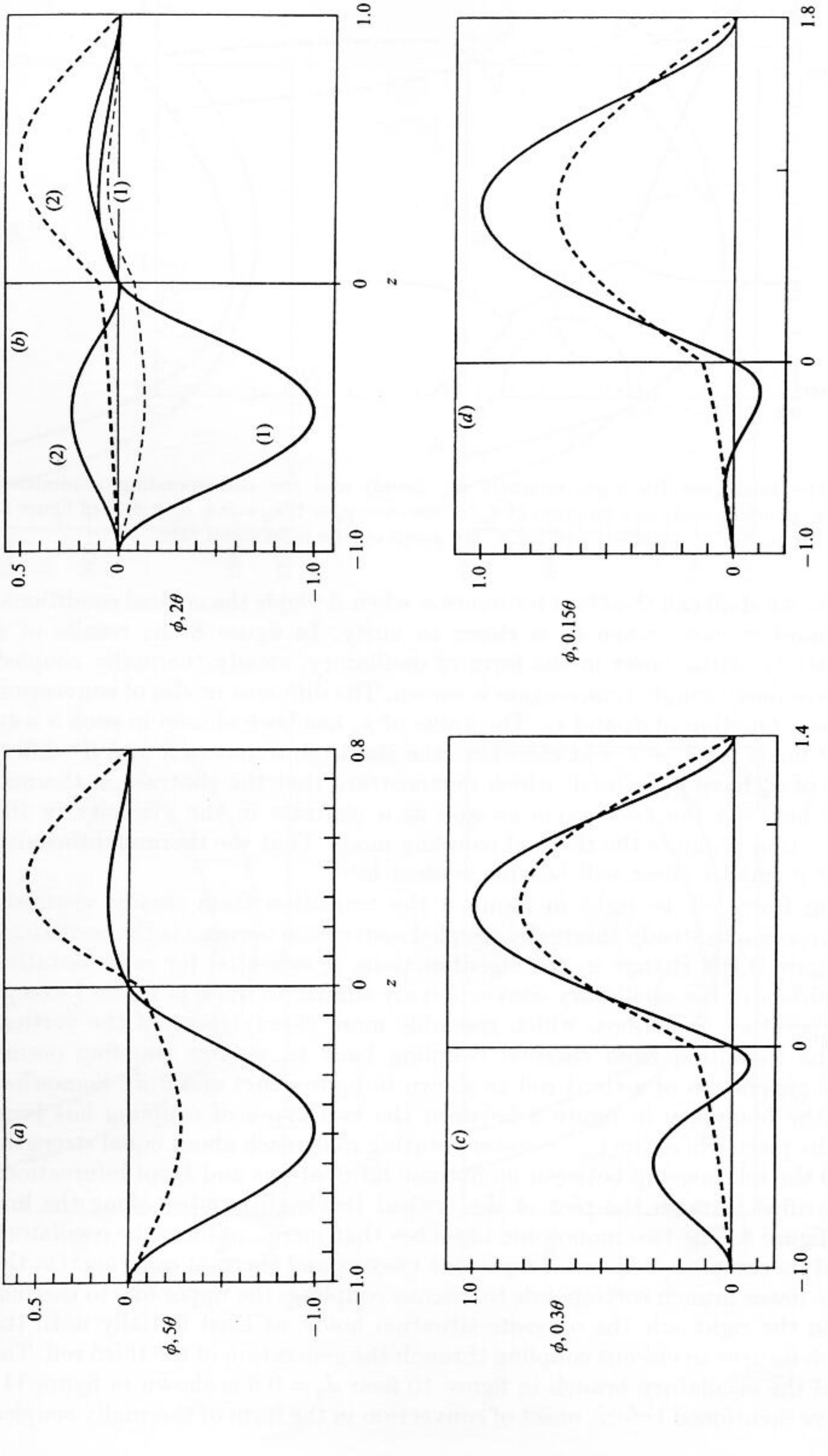

FIGURE 9. Eigenfunctions $\phi(z)$ (solid) and $\theta(z)$ (dashed) for the case $\gamma_0 = 0.25$, $\kappa_0 = 0.2$ of figure 8. The functions are shown for (*a*) $d_0 = 0.8$, (*b*) 1.0, (*c*) 1.4 and (*d*) 1.8. In (*b*) the curves (1) and (2) are a quarter of a cycle apart.

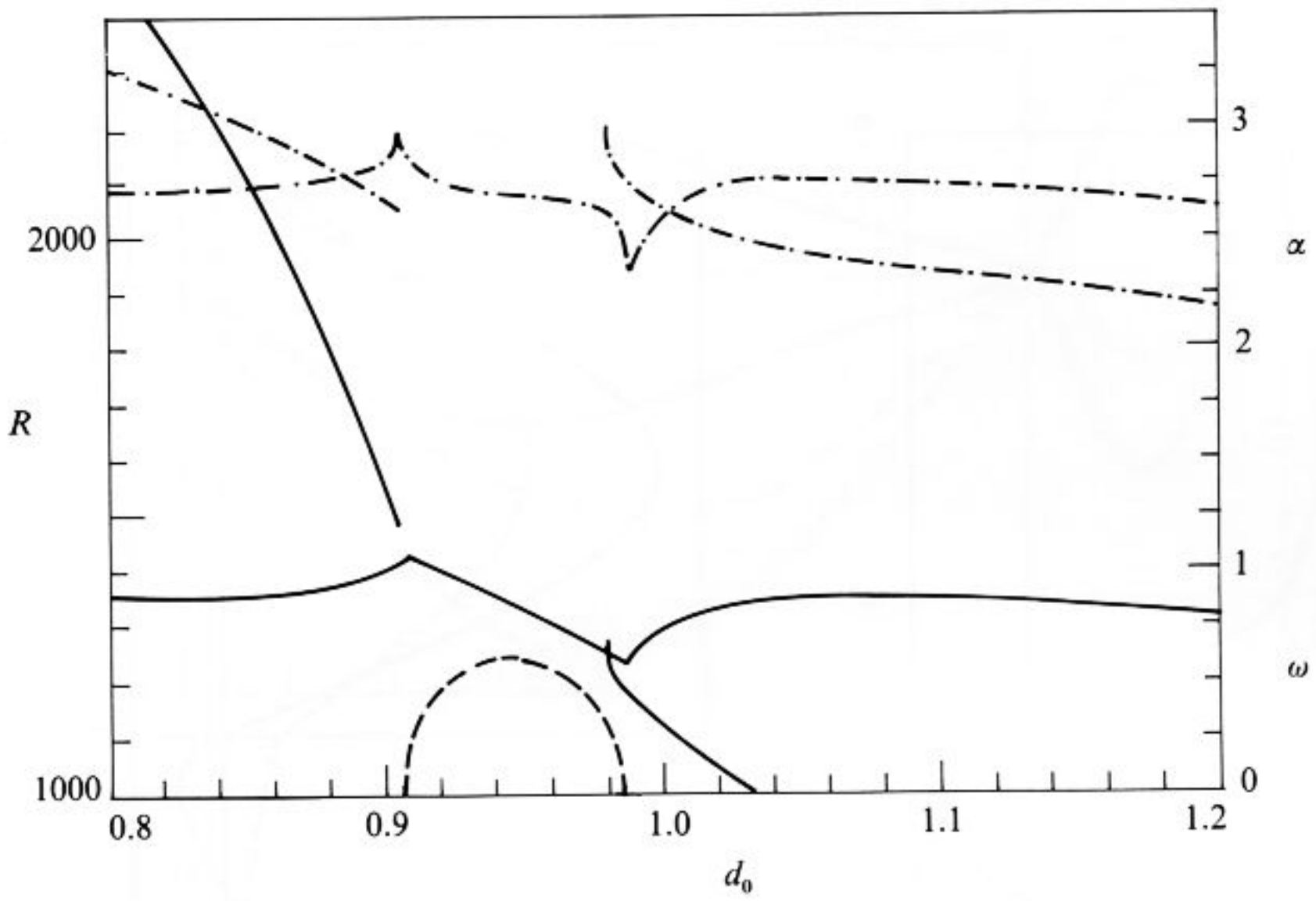

FIGURE 10. The minimum Rayleigh numbers R_m (solid) and the corresponding minimizing wavenumber α_c (dash-dotted) as a function of d_0 for the case $\gamma_0 = 1$, $\kappa_0 = 0.4$, $\mu_0 = 6.25$ of figure 8. Scales for the frequency ω_c (dashed) and for α_c are given on the right-hand side.

instability, as we shall call the Hopf bifurcation when it yields the critical conditions, is indeed found in cases when d_0 is closer to unity. In figure 8 the results of a systematic study of the onset in the form of oscillatory, steady thermally coupled and steady viscously coupled convection is shown. The different modes of convection are shown as a function of d_0 and κ_0. The value of μ_0 has been chosen in such a way that $R = R^*$ holds for $d_0 = 1$; but elsewhere the Rayleigh numbers R and R^* differ. Two values of γ_0 have been used, which demonstrate that the contrast in thermal expansivity between the two layers as well as a contrast in the viscosity in the opposite direction promote the thermal coupling mode. That the thermal diffusivity contrast has a smaller effect will become evident later.

In moving from left to right in figure 8 the transition from steady viscously coupled convection to steady thermally coupled convection occurs via the oscillatory mode. In figure 9 the change in the eigenfunctions is indicated for representative cases. The phases of the oscillatory convection are similar to those of figure 7 except for the temperature variations, which resemble more closely those of the vertical velocity. The transition from thermal coupling back to viscous coupling occurs through the generation of a third roll as shown in figures 9(*c*) and 9(*d*). Somewhat arbitrarily the boundary in figure 8 between the two types of coupling has been defined as the place where the two counter-rotating rolls reach about equal strength. In figure 10 the relationship between monotonic bifurcations and Hopf bifurcations becomes clarified through the plot of the critical Rayleigh number along the line $\kappa_0 = 0.4$ of figure 8. The two monotonic branches that merge to form the oscillatory branch (and its complex conjugate) represent viscous and thermal coupling. On the left side, the lower branch corresponds to viscous coupling, the upper one to thermal coupling; on the right side the opposite situation holds, at least initially until the lower branch returns to viscous coupling through the generation of the third roll. The evolution of the oscillatory branch in figure 10 near $d_0 = 0.9$ is shown in figure 11.

As we have mentioned before, onset of convection in the form of thermally coupled

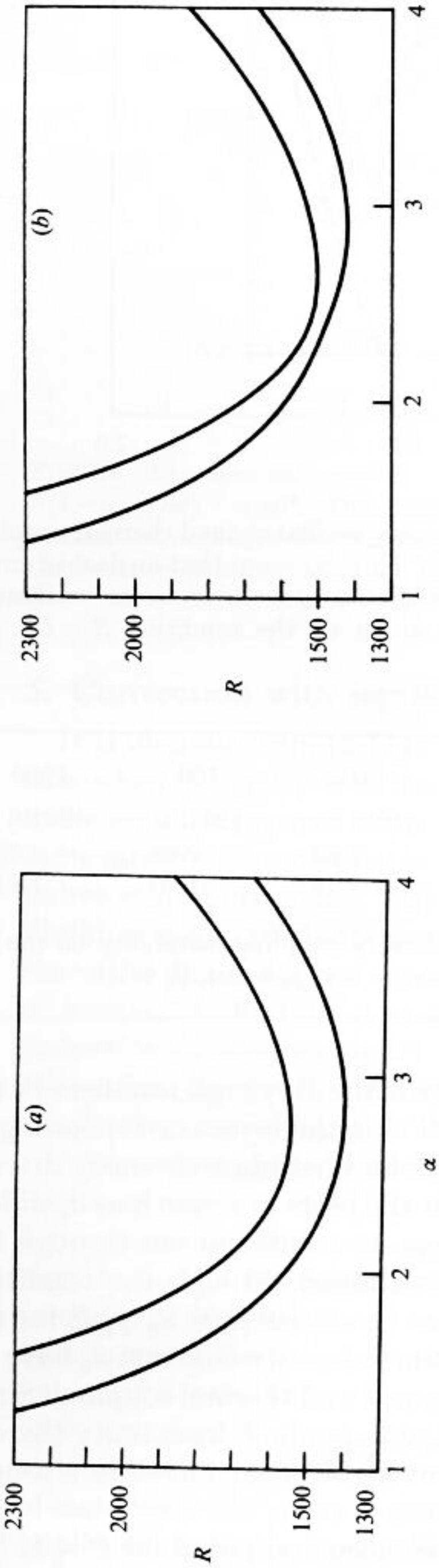

FIGURE 11. The evolution of the oscillatory branch in figure 10 near $d_0 = 0.9$. The two monotonic branches and the Hopf branch of the Rayleigh number $R(\alpha)$ are shown for different values of d_0. The dashed curve indicates the frequency ω which is measured on the right ordinate. (*a*) $d_0 = 0.900$, (*b*) 0.904, (*c*) 0.905, (*d*) 0.910.

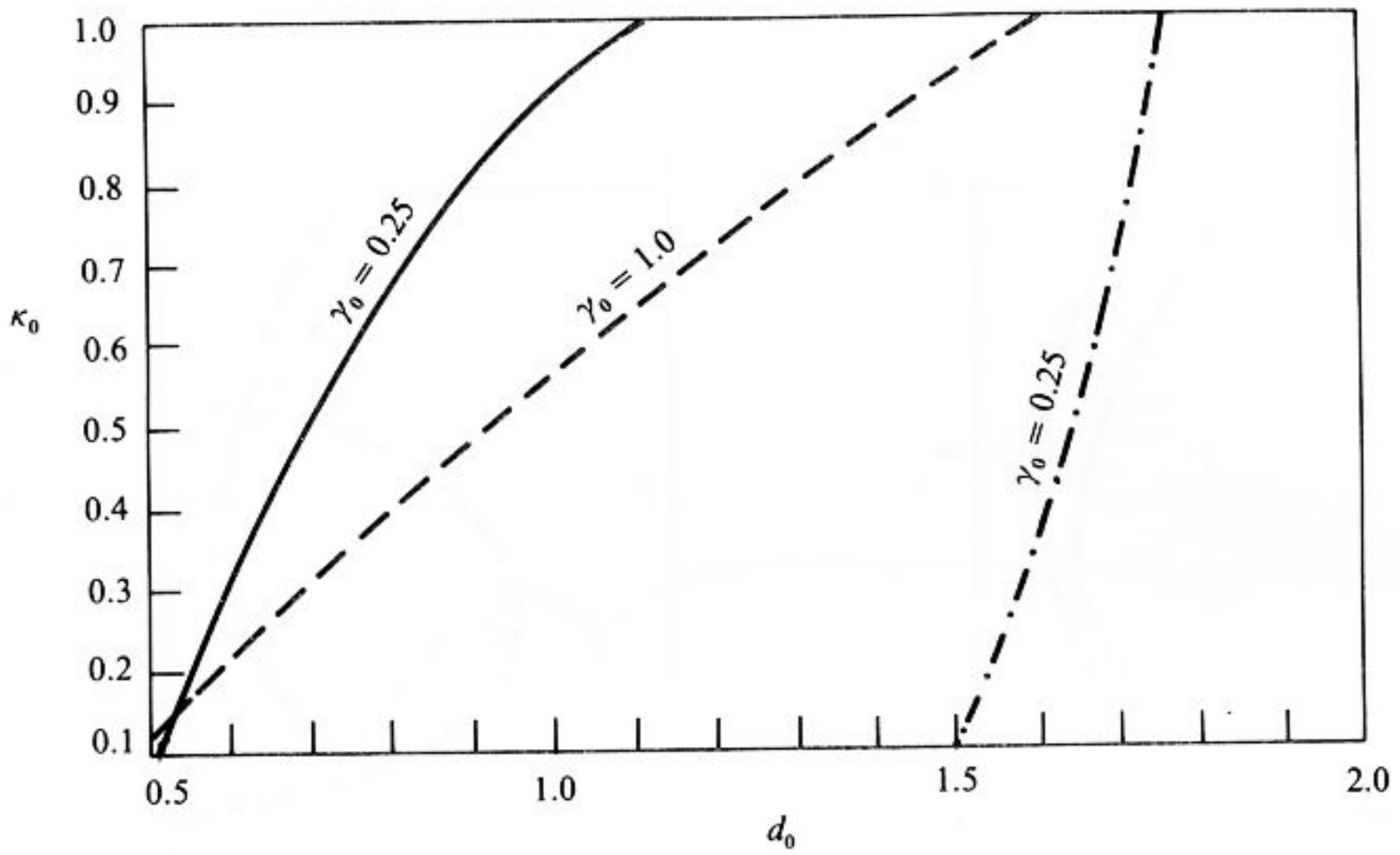

FIGURE 12. Approximate boundaries between regimes of viscous, oscillatory and thermal coupling in the case $\gamma_0 = 0.25$. The boundaries follow the description of figure 8 except that no dashed curve appears. In the present figure the dashed curve describes the case $\gamma_0 = 1.0$ where no oscillatory instability has been found. In contrast to figure 8, μ_0 is given by the condition $R = R^*$, i.e. $\mu_0 = \kappa_0^{-2}\gamma_0^0 d_0^4$.

P	0.001	0.01	0.1	1	10	100	1000
R_c	1191.3	1190.8	1189.8	1197.2	1201.0	1201.6	1201.6
α_c	2.61	2.70	2.647	2.63	2.63	2.63	2.63
ω_c	0.0074	0.072	0.437	1.001	1.18	1.20	1.21

TABLE 1. Dependence of critical parameters of the oscillatory coupling instability on the Prandtl number P in the case $d_0 = 1$, $\mu_0 = 3.125$, $\kappa_0 = 0.4$, $\gamma_0 = 0.4$, $\gamma_0 = 0.5$

motions or oscillatory motions can be expected only if the Rayleigh numbers in the two layers are not very different. Otherwise convection in the layer corresponding to the lower value among R and R^* plays a passive role and becomes viscously driven. For this reason viscous coupling becomes the rule in the plots of figure 8 as d_0 differs sufficiently markedly from unity. This property suggests a different cut through the parameter space of the problem in which μ_0 is determined through the condition $R = R^*$ for all d_0. Instead of $\mu_0 = \kappa_0^{-2}\gamma_0$, as in figure 8, we use $\mu_0 = \kappa_0^{-2}\gamma_0 d_0^4$ for the diagram of figure 12. In this figure the lines of constant viscosity contrast μ_0 have an inclination similar to that of the curve separating viscous and thermal coupling. Since viscous coupling becomes rather ineffective when μ_0 differs much from unity there is no return to viscously coupled convection with growing d_0 as μ_0 increases strongly with d_0.

All frequencies shown in figures 6, 10 and 11 have been computed for $P = 1$. For larger values of the Prandtl number, Rayleigh numbers and frequencies change very little, but for small P the frequency ω_c varies proportionally to P as is evident from table 1. This behaviour indicates that the sum of the viscous and the thermal timescales determines the period of the oscillatory coupling instability, as must be expected on the basis of the physical mechanism discussed above.

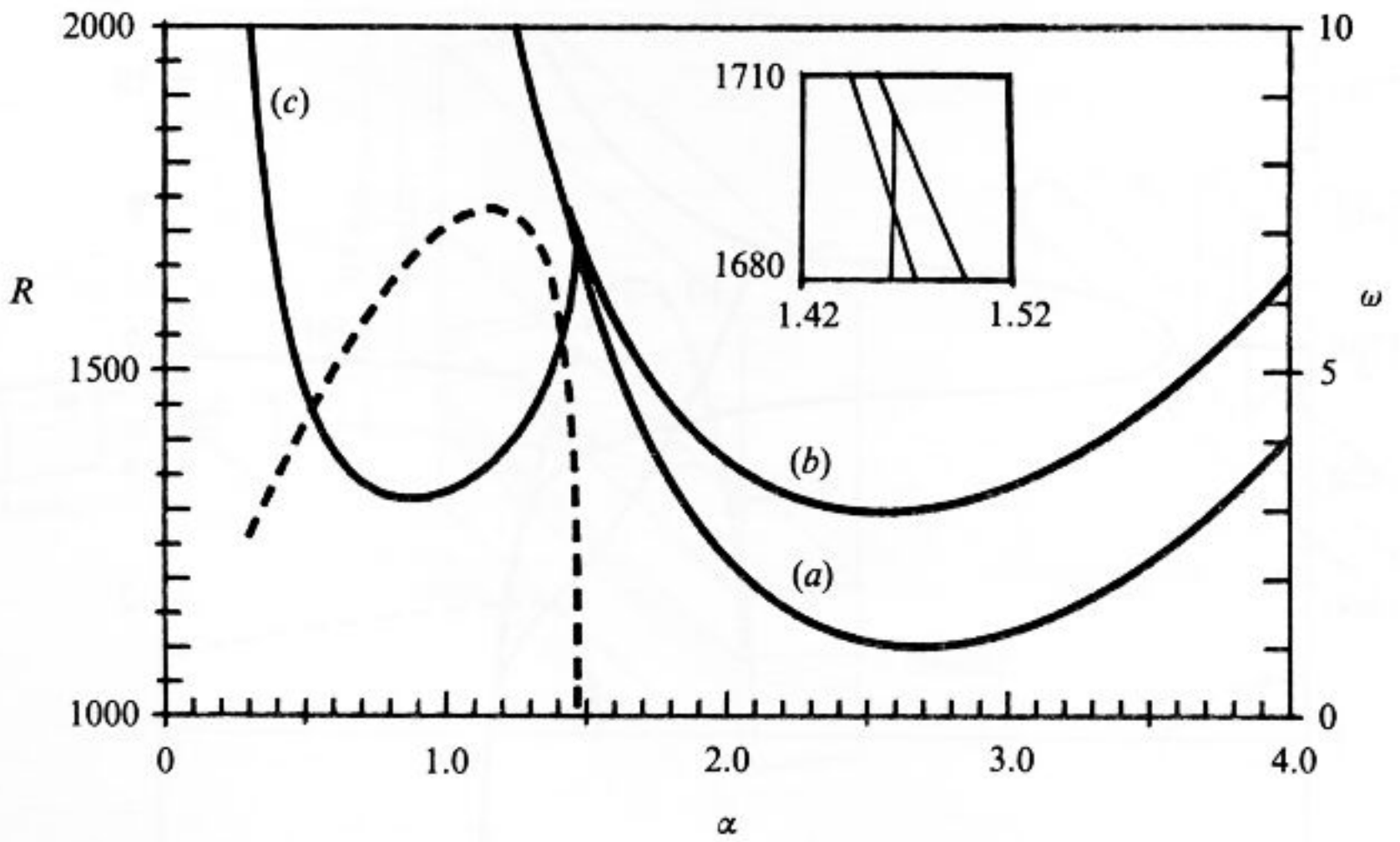

FIGURE 13. Neutral curves $R(\alpha)$ for the case $\gamma_0 = d_0 = \kappa_0 = \mu_0 = P = 1$ with $R = R^*$, $R(1-\rho_0)(\gamma\beta d)^{-1} = 10^3$. The dashed curve (*right scale*) indicates the frequency of the Hopf bifurcation curve (*c*). The curves (*a*), (*b*) correspond closely to the curves of figure 2. The details near the codimension-two point are shown in the inset figure.

5. Convection with significant distortion of the interface

It is obvious from (2.11*f*) that the distortion ζ_0 can enter the problem only in the case when $(\rho-\rho^*)/\rho$ is of the same order as $\gamma\beta d$. Since the latter quantity is assumed to be small compared with unity according to the Boussinesq approximation the same must be assumed for $(\rho-\rho^*)/\rho$, where $\rho^* < \rho$ is supposed to hold in the following unless stated otherwise. For this reason the calculations mentioned by Gershuni & Zhukhovitskii (1976) are not entirely consistent with the Boussinesq approximation. Since the dimensionless surface tension S is of the order 10^5 for many combinations of immiscible liquids, it is not easy to obtain laboratory situations in which the distortion ζ_0 becomes significant. Special surfactants may have to be used to reduce the surface tension of immiscible liquids. For simplicity we shall restrict attention to the limit of vanishing S in the following.

An example of the oscillatory instability with distortion is given in figure 13. Two layers of equal properties have been chosen. The curves (*a*, *b*) for monotonic bifurcations are the same as those shown in figure 2 except that they are shifted to slightly higher Rayleigh numbers. The oscillatory mode, however, depends on the presence of the distortion and the eigenfunction for the vertical velocity reaches a maximum at the interface throughout almost the entire cycle. We have chosen the value 10^3 for the ratio $(1-\rho_0)R/\gamma\beta d$ which depends only on the material properties of the two liquids. For higher values of this ratio the curve (*c*) in figure 13 would move up and the curves (*a*, *b*) would move even closer to those of figure 2. The mechanism of instability obviously depends on the approximate inequality $\gamma\beta d > (1-\rho_0)$ which implies that the density of the bottom half of the lower layer is lower than the density in the top half of the upper layer in spite of the stabilizing density jump across the interface. The oscillatory character of the instability indicates that a Rayleigh–Taylor type overturning instability operates throughout part of the cycle, while dissipative effects together with the stabilizing density contrast across the interface lead to a restoring force throughout the remainder of the cycle. The name 'oscillatory

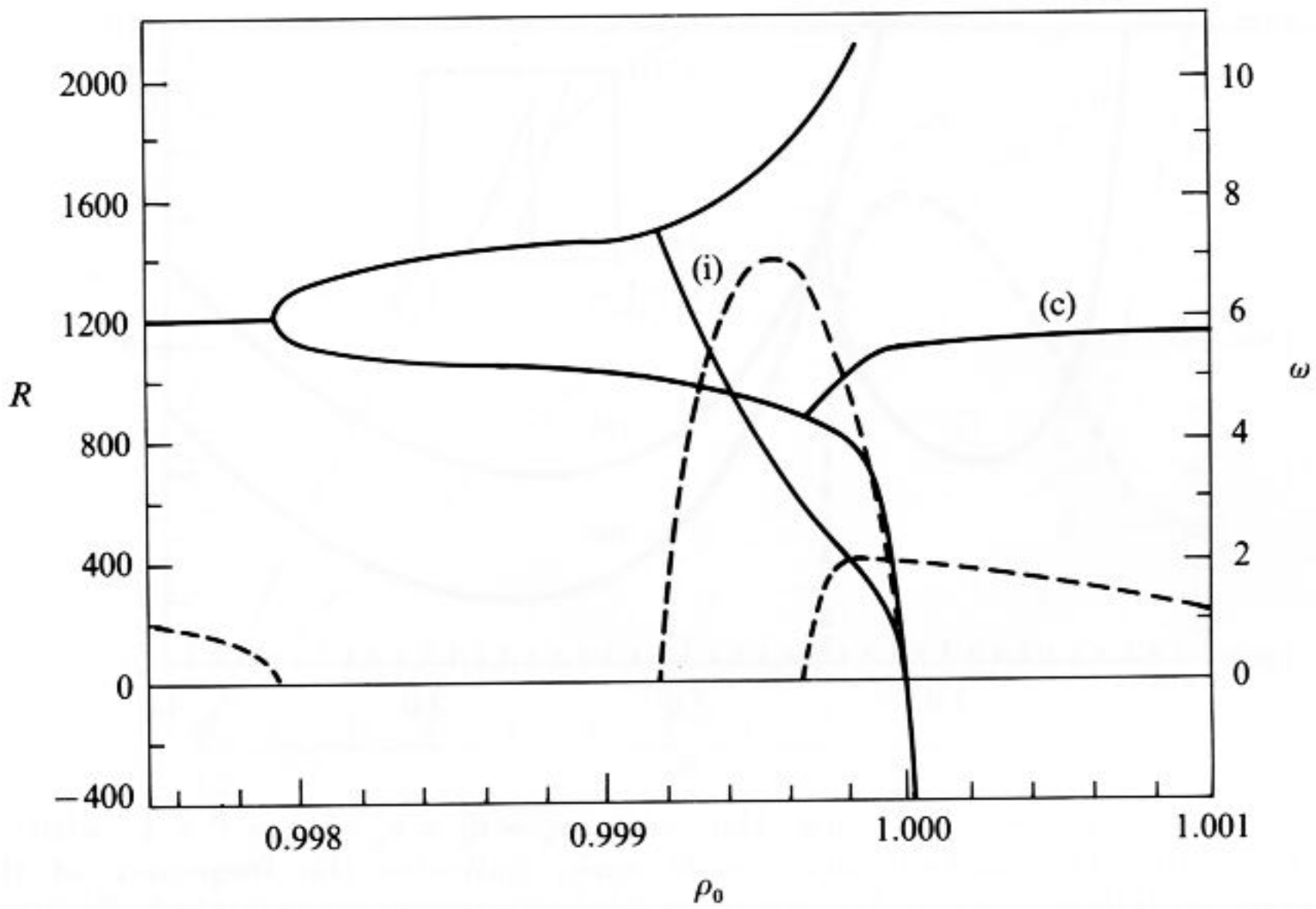

FIGURE 14. The Rayleigh number as a function of ρ_0 in the case $d_0 = P = 1$, $\gamma_0 = 0.5$, $\kappa_0 = 0.4$, $\mu_0 = 3.125$, $\alpha = 2.6$, $R(\gamma\beta d)^{-1} = 10^6$. The wavenumber $\alpha = 2.6$ has been chosen because it corresponds to the critical value in the case $\zeta_0 \equiv 0$. The dashed lines (measured on the right ordinate) indicate the frequencies of the oscillatory interfacial (i) and the oscillatory coupling (c) instabilities.

interfacial instability' seems to be appropriate to distinguish this instability from the oscillatory coupling instability.

In order to study the influence of the new parameter $1-\rho_0$ on the problem we choose a case for which the critical Rayleigh number corresponds to the onset of the oscillatory coupling instability in the limit $\zeta_0 \equiv 0$. Indeed, as is shown in figure 14, this limit with $R_c \approx 1200$, $\omega = 1$ is approached as $|1-\rho_0|$ becomes of the order 3×10^{-3} or larger. As $1-\rho_0$ decreases to 2×10^{-3} the frequency vanishes and the oscillatory mode and its complex conjugate change into two monotonic modes. The one with the lower Rayleigh number is characterized by viscous coupling, the other by thermal coupling. As $1-\rho_0$ decreases further to less than 10^{-3} the oscillatory interfacial mode bifurcates from the thermal coupling branch. It joins the viscous coupling branch at the point $R = 0$, $\rho_0 = 1$, where the frequency vanishes again. The point $R = 0$, $\rho_0 = 1$ determines, of course, the onset of the Rayleigh–Taylor instability, which is independent of the wavenumber α in the limit of vanishing surface tension S that we have assumed. The merger with the Rayleigh–Taylor mode emphasizes again the importance of the distortion in the oscillatory interfacial instability first found by Richter & Johnson (1974).

Before $1-\rho_0$ reaches zero from above the oscillatory coupling mode bifurcates from the viscous coupling branch. Its frequency increases rapidly and decreases later towards the value $\omega_0 = 1$ which characterizes the problem without distortion. The oscillatory coupling mode may have physical importance only if the surface tension is strong enough and low values of α are prohibited by the geometry of the layer such that the Rayleigh–Taylor instability is stabilized. In the case of figure 14 the Rayleigh–Taylor instability represents a very strong mechanism such that neutral conditions are reached only at $R = -1.89\times10^6$ when $\rho_0 - 1$ is as small as 10^{-3}.

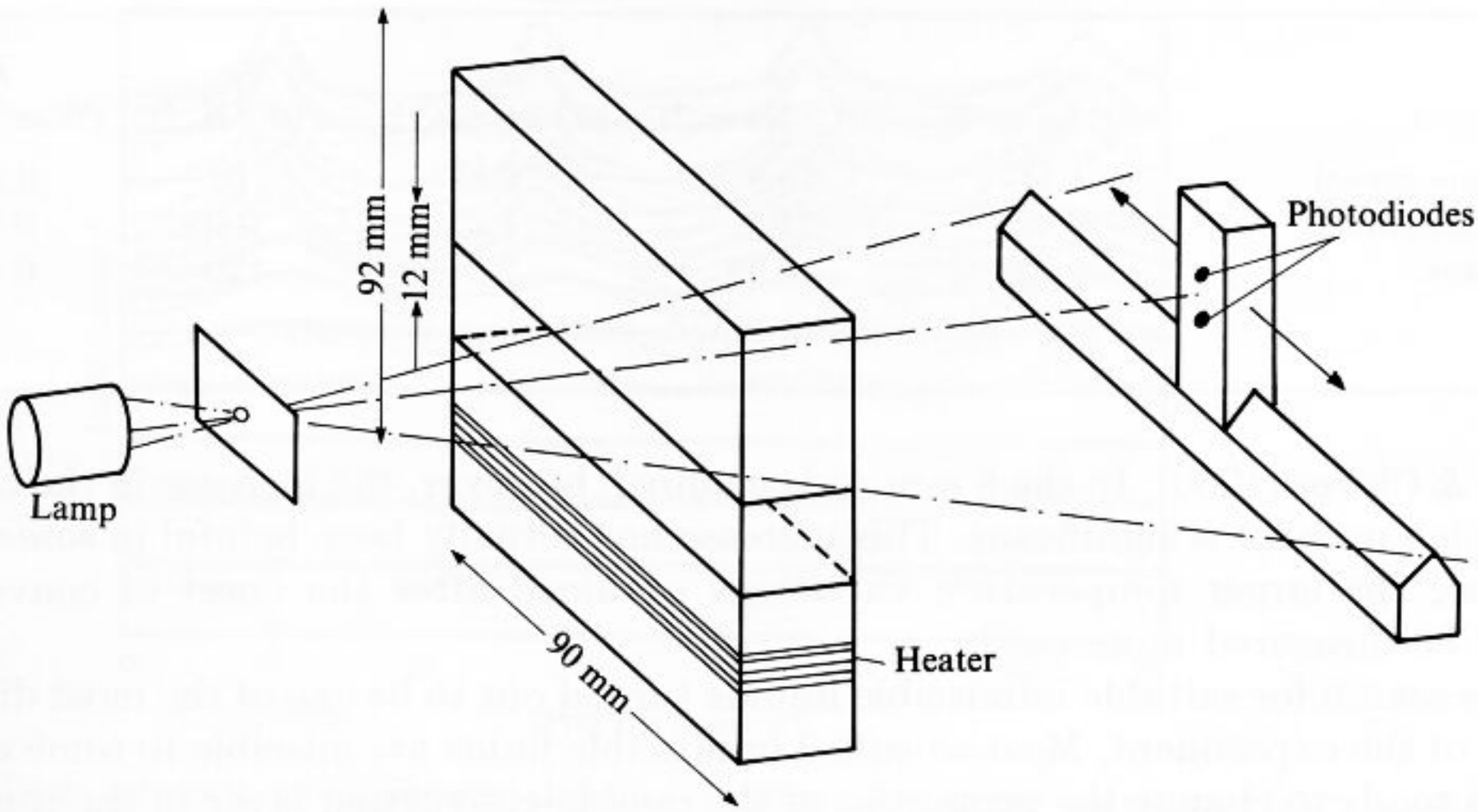

FIGURE 15. Schematic diagram of the experimental apparatus and method of observation.

6. Experimental apparatus for the study of double-layer convection

In order to compare the theoretical predictions with experimental observations a convection layer in the form of a channel sandwiched between two copper blocks has been built as shown in figure 15. The form of a horizontal channel has been chosen in order to force alignment of the convection rolls parallel to the short side of the channel. The pattern of convection was observed with the shadowgraph method. Parallel light intersecting the channel along the axis of the rolls is slightly deflected because of the varying index of refraction. The light intensity received on the other side of the channel thus measures the change in the index of refraction and thereby the horizontal distribution of the temperature. A camera was used to obtain a picture of the variations in light intensity or alternatively a photo diode was moved in parallel to the long side of the channel by a stepping motor and a curve measuring the light intensity at a certain height of the channel was obtained. Here we shall report only results obtained with the latter technique.

Two different channels with the dimensions $90 \times 20 \times 12$ mm^3 and $140 \times 8 \times 12$ mm^3 were used, where 12 mm refers to the height d of the channel. The sidewalls were made from 1 mm thick glass and the lower copper block was heated by a 50 Ω resistance wire of constantin. A water cooling channel kept the upper copper block at a constant temperature. The system was enclosed in a box which itself was insulated by styrofoam. The temperature difference between the copper blocks in the neighbourhood of the boundary of the convection layer was measured with several copper–constantin thermo-elements. The accuracy of the temperature measurements was better than 0.01 K; the accuracy to which the temperature difference between top and bottom of the channel could be kept constant over periods of the order of hours was 0.03 K.

The height of the channel was chosen sufficiently large such that the uncertainty in the position of the interface caused by the meniscus is relatively small, while the temperature difference across the layer is not too small for the selected liquids. In the case of the 20 mm wide channel the influence of the sidewalls on the critical Rayleigh number is sufficiently small to be negligible according to the theoretical results of

	ρ (10^3 kg m^{-3})	μ (10^{-3} Ns m^{-2})	c_p (kJ kg^{-1} K^{-1})	γ (10^{-5} K^{-1})	λ (Wm^{-1} K^{-1})
Ethylene glycol	1.11	19.9	2.35	62	0.25
Oil [Hanseline®]	0.90	23.8	1.8	100	0.15
n-Decane	0.73	0.93	2.2	120	0.13

TABLE 2. Properties of liquids used in experiments

Frick & Clever (1980). In the 8 mm wide channel, however, the increase in the critical Rayleigh number is significant. This increase has actually been helpful in some cases because the larger temperature variations obtained after the onset of convection could be measured more easily.

The search for suitable immiscible liquids turned out to be one of the most difficult tasks of the experiment. Most so-called immiscible fluids are miscible to some extent which tends to change the properties of the double-convection layer in the course of an experimental run. This problem is amplified by the temperature dependence of solubility which could, for example, cause separation of the mixed phase at the cold boundary. From the observational point of view it is also desirable that the variation in the index of refraction induced by convection is comparable for both liquids. The combinations ethylene glycol–oil and ethylene glycol–decane were finally selected because of the miscibility of less than 0.1% and because of a relatively small difference in the adhesion to the glass wall. The oil is actually a commercially available mixture (Hanseline®) the properties of which had to be measured. Since the coefficient of expansion, the thermal conductivity and the specific heat do not vary much for different mineral oils, the typical values listed in handbooks such as Hodgman (1960) have been used. The properties are listed in table 2. The temperature dependence of the surface tension has not been included since the Marangoni effect was small in comparison with the buoyancy effect in the experimental configuration.

In the case of the oil a temperature gradient can induce variations in the concentrations of the constitutents of the oil. In order to avoid this Soret effect, the experiments have to be carried out on a timescale that is sufficiently short in comparison with the timescale of diffusion. Alternatively, the Rayleigh number for onset of convection can be determined by decreasing the Rayleigh number rather than by increasing it. In this fashion the mixing by the convection motion overcomes the Soret effect. The experimental runs reported in the next section have been done using both methods and have not led to any significant difference in the results.

7. Experimental observations

A typical record of an experimental run is shown in figure 16. The Rayleigh number R^* is about 30% higher in this case than R. Convection predominates in the upper layer at Rayleigh numbers beyond the critical value for onset of convection until the variation of temperature becomes clearly noticeable in the lower layer as well. The relative phase of the temperature signal indicates thermal coupling. In figure 17 this experimental run has been repeated in the 8 mm wide channel. Now the weak variation of the temperature in the lower layer after onset of convection can be resolved which indicates viscous coupling before the transition to thermal coupling. The theoretical analysis agrees with these observations. The predicted onset

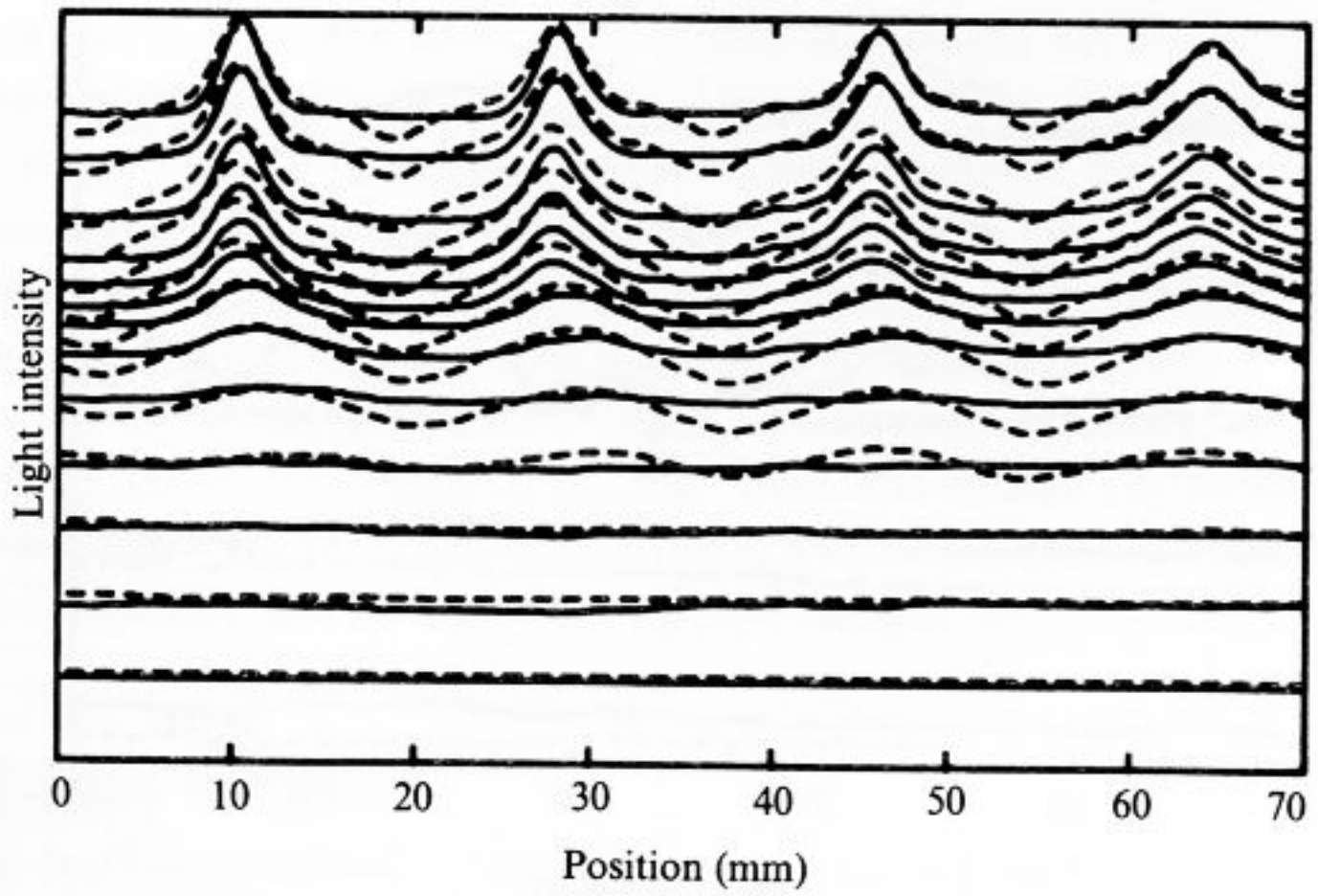

FIGURE 16. Light intensity along horizontal tracks corresponding to the lower layer (glycol, solid line) and to the upper layer (oil, dashed line) for the 2 cm wide channel with $d_0 = 1$. The lines correspond to the temperature differences (from the bottom) 1.38 K, 1.77 K, 2.12 K, 2.47 K, 2.77 K, 3.09 K, 3.41 K, 3.74 K, 4.05 K, 4.36 K, 4.61 K, 4.85 K, 5.09 K.

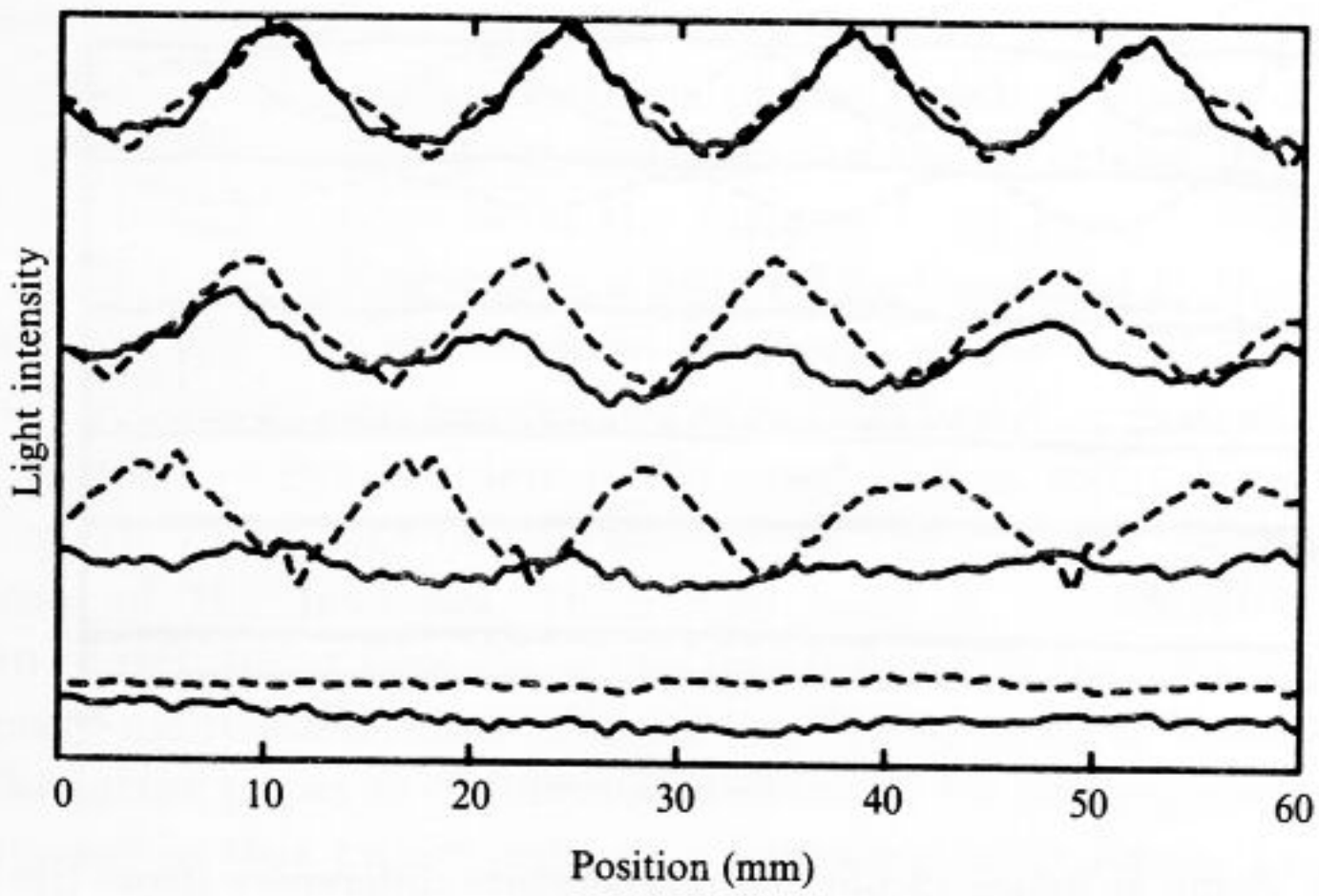

FIGURE 17. Same as figure 16, except for a 0.8 cm wide channel. The temperature differences (from the bottom) are 3.40 K, 4.07 K, 4.66 K, 5.26 K.

occurs at $\Delta T = 2.22$ K while the observed value for the 20 mm wide channel is $\Delta T = 2.1 \pm 0.2$ K. The theoretical analysis indicates a second Rayleigh number as in figure 2 corresponding to thermal coupling. Although a nonlinear analysis is needed to follow the evolution of finite-amplitude convection, the linear analysis is useful in this case since thermal coupling usually seems to win in the competition between the two types of coupling. Even the theoretically predicted decrease in the critical wavenumber of about 5% in the transition from the viscous to the thermal coupling case seems to be borne out by the experiment. An increase of the wavelength is clearly noticeable both in figure 16 and in figure 17.

In a second series of experiments the glycol layer has been increased in size such that the case $d_0 = 0.7$ is attained. Because of the relationship $R > R^*$ the wavelength of 27 mm at the onset of convection reflects the size of the deeper layer as shown in

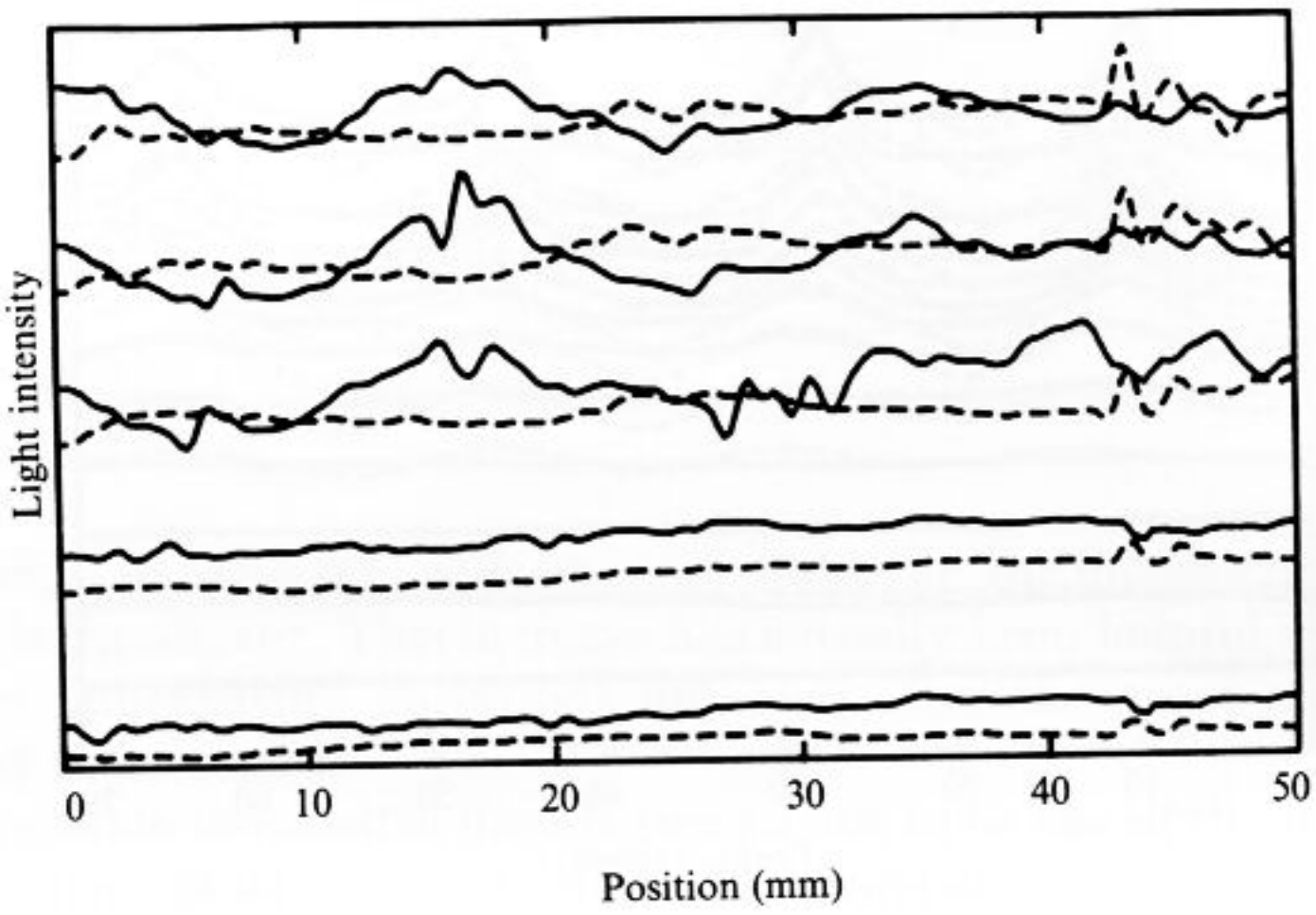

FIGURE 18. Same as figure 16, but for $d_0 = 0.71$. The temperature differences (from the bottom) are 2.01 K, 2.18 K, 2.29 K, 2.47 K, 2.60 K.

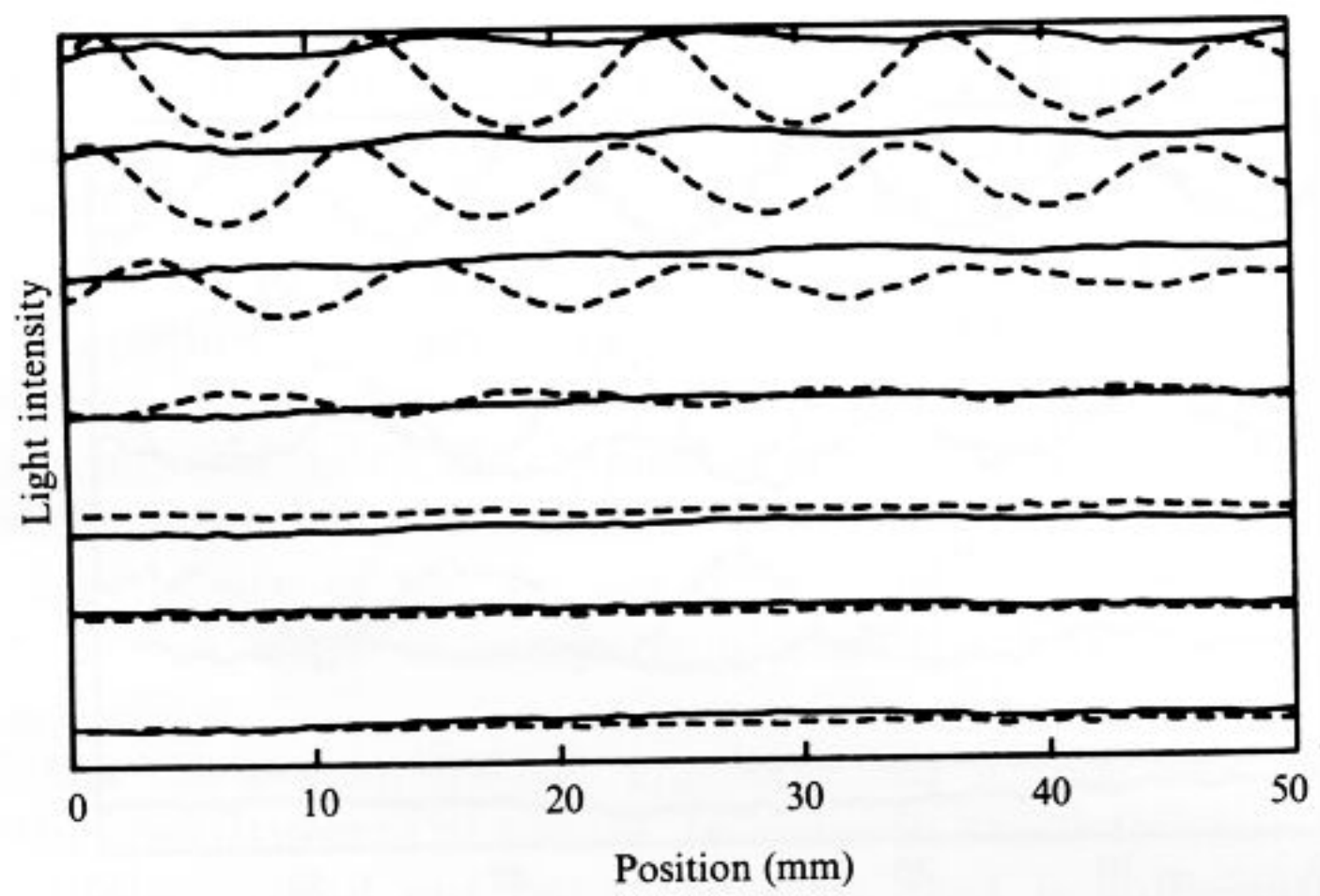

FIGURE 19. Same as figure 18 but the temperature differences (from the bottom) are 3.69 K, 3.89 K, 4.13 K, 4.34 K, 4.52 K, 4.73 K, 4.90 K.

figure 18. Because of the weak signal, a high amplification has been used in recording the light intensity. The signal-to-noise ratio is thus much lower than in the previous figures. The critical temperature difference of 2.1 ± 0.2 K obtained from the data of figure 18 and from similar data agrees well with the theoretical value of 2.14 K. The viscous coupling evident in figure 18 persist until a temperature difference of 3.3 K is reached, at which point a convection mode with its maximum amplitude in the upper layer starts to compete with the existing convection structure. No regularly arranged convection could be observed in the interval $3.3\ \mathrm{K} \lesssim \Delta T \lesssim 4.1\ \mathrm{K}$. There appear to be adjustment difficulties which prohibit the system from selecting a well-organized state. At $\Delta T = 4.3$ K, however, the upper-layer mode appears to become dominant and a well-defined pattern with a wavelength of 12 mm becomes visible as shown in figure 19. The layers are thermally coupled in this regime; the small phase shift between the solid and broken lines in the upper part of the figure is caused by a slow drift of the pattern. Because of the non-uniform adhesion of the interface to

the glass walls it was not always possible to obtain an exactly horizontal interface. A slow large-scale circulation is thus sometimes present which appears to be responsible for the drift of the pattern that becomes noticeable on the timescale of 15 minutes, the interval between the recording of the solid and broken lines.

The observations in the glycol–decane system show rather similar results which will not be reported here, but can be found in Rasenat (1987). One of the main goals, the observation of the oscillatory onset of convection, has not yet been achieved. An experimental search is continuing. But because of the restricted types of immiscible liquids available and the time-consuming experimental procedure there is little hope that the oscillatory onset can be realized in the near future.

8. Concluding remarks

In principle numerical computations carried out at particular points of the parameter space do not permit rigorous global conclusions about the behaviour of solutions as a function of the parameters. This restriction is felt most strongly in the case of high-dimensional parameter spaces such as that associated with the problem of double-layer convection considered in this paper. Because of space limitations only representative examples of the computations that have been performed in the course of this work have been described in the preceding sections. It seems, however, that all the physically interesting features of the onset of double-layer convection have been covered in the case without distortion of the interface. The main results are that onset of convection can occur in the form of both viscously and thermally coupled motion and that a Hopf bifurcation noticed by Gershuni & Zhukhovitskii (1982) does indeed describe the critical mode in the form of the oscillatory coupling instability in a certain region of the parameter space. When the distortion of the interface is included, a much richer problem is obtained and an extra time derivative enters the analysis together with one or two additional parameters. Because of the geophysical implications of the problem, there has been a considerable effort in numerical simulation of nonlinear aspects of the problem. Other relevant papers, in addition to those already mentioned, are Busse (1982), Christensen & Yuen (1984) and Schmeling (1988). The latter paper is of particular interest for the regime $\rho_0 > 1$, $R < 0$ that has been discussed in this paper only in connection with figure 14.

Even without its geophysical applications the problem of double-layer convection is likely to attract continuing and increasing attention. The numerous bifurcation features already apparent in the linear theory will lead to an even richer variety of structures when nonlinear regimes are considered. The possibility of different spatial patterns in the upper and lower layers opens up new degrees of freedom in nonlinear interaction. The recent work by Cserepes, Rabinowicz & Rosenburg-Borot (1988) on three-dimensional double-layer convection gives some indications of those possibilities. Detailed experimental observations and measurements are especially desirable in the current state of the research on this problem.

The support of the Stiftung Volkswagenwerk for the research reported in this paper is gratefully acknowledged.

REFERENCES

Busse, F. E. 1981 On the aspect ratio of two-layer mantle convection. *Phys. Earth Planet. Interiors.* **24**, 320–324.

Busse, F. H. 1982 Multiple solutions for convection in a two component fluid. *Geophys. Res. Lett.* **9**, 519–522.

Christensen, U. R. & Yuen, D. A. 1984 The interaction of a subducting lithospheric slab with a chemical or phase boundary. *J. Geophys. Res.* **89**, 4389–4402.

Cserepes, L. & Rabinowicz, M. 1985 Gravity and convection in a two-layer-mantle. *Earth Planet. Sci. Lett.* **76**, 193–207.

Cserepes, L., Rabinowicz, M. & Rosemberg-Borot, C. 1988 Three-dimensional convection in a two-layer mantle. *J. Geophys. Res.* (submitted).

Ellsworth, K. & Schubert, G. 1985 Two-layer convection in the earth mantle, *EOS Trans. Am. Geophys. Union* **66**, 1070.

Frick, H. & Clever, R. M. 1980 Einfluß der Seitenwände auf das Einsetzen der Konvektion in einer horizontalen Flüssigkeitsschicht *Z. Angew. Math. Phys.* **31**, 502–513.

Gershuni, G. Z. & Zhukhovitskii, E. M. 1976 *Convective Stability of Incompressible Fluids* (Translated from the Russian by D. Louvish). Jerusalem: Keter Publications.

Gershuni, G. Z. & Zhukhovitskii, E. M. 1982 Monotonic and oscillatory instabilities of a two-layer system of immiscible liquids heated from below. *Sov. Phys. Dokl.* **27**, 531–533.

Hodgman, C. D. (ed.) 1960 *Handbook of Chemistry and Physics*, 42nd edn. Cleveland, Ohio: The Chemical Rubber Publishing Co.

Nguyen, A. T. & Kulacki, F. A. 1980 Convection in multi-layer systems. In *Mechanisms of Continental Drift and Plate Tectonics* (ed. P. A. Davis & S. K. Runcorn), pp. 259–266. Academic.

Pellew, A. & Southwell, R. V. 1940 On maintained convective motion in a fluid heated from below. *Proc. R. Soc. Lond.* A **176**, 312–343.

Proctor, M. R. E. & Jones, C. A. 1988 The interaction of two spatially resonant patterns in thermal convection, I. Exact 1:2 resonance. *J. Fluid. Mech.* **188**, 301–335.

Rasenat, S. 1987 Konvektion in zwei geschichteten Flüssigkeiten. Diploma thesis, Institute of Physics, University of Bayreuth.

Renardy, Y. & Joseph, D. D. 1985 Oscillatory instability in a Bénard problem of two fluids. *Phys. Fluids* **28**, 788–793.

Renardy, Y. & Renardy, M. 1985 Perturbation analysis of steady and oscillatory onset in a Bénard problem with two similar liquids. *Phys. Fluids* **28**, 2699–2708.

Richter, F. M. & Johnson, G. E. 1974 Stability of a chemically layered mantle. *J. Geophys. Res.* **79**, 1635–1639.

Schmeling, H. 1988 Numerical models of Rayleigh–Taylor instabilities superimposed with convection. Preprint, Institute of Geology, Uppsala University.

Zeren, R. W. & Reynolds, W. C. 1972 Thermal instabilities in two-fluid horizontal layers. *J. Fluid Mech.* **53**, 305–327.